

# Thermal runaway propagation model for designing a safer battery pack with 25 Ah $\text{LiNi}_x\text{Co}_y\text{Mn}_z\text{O}_2$ large format lithium ion battery

Xuning Feng<sup>a</sup>, Xiangming He<sup>b</sup>, Minggao Ouyang<sup>a,\*</sup>, Languang Lu<sup>a</sup>, Peng Wu<sup>c</sup>, Christian Kulp<sup>c</sup>, Stefan Prasser<sup>c</sup>

<sup>a</sup> State Key Laboratory of Automotive Safety and Energy, Tsinghua University, Beijing 100084, China

<sup>b</sup> Institute of Nuclear and New Energy Technology, Tsinghua University, Beijing 100084, China

<sup>c</sup> BMW China Services Ltd., Beijing 100027, China

## HIGHLIGHTS

- A lumped thermal runaway (TR) propagation model for Li-ion battery pack is built.
- The TR propagation model can fit experimental results well.
- Modeling analysis of the parameters helps find solutions to prevent TR propagation.
- Quantified solutions to prevent TR propagation in Li-ion battery pack are provided.
- TR propagation mechanism in a large format Li-ion battery pack is revealed.

## ARTICLE INFO

### Article history:

Received 8 January 2015

Received in revised form 10 March 2015

Accepted 28 April 2015

Available online 14 May 2015

### Keywords:

Lithium ion battery

Safety

Thermal runaway

Thermal runaway propagation

Propagation prevention

## ABSTRACT

Thermal runaway (TR) propagation in a large format lithium ion battery pack can cause disastrous consequences and thus deserves study on preventing it. A lumped thermal model that can predict and help prevent TR propagation in a battery module using 25 Ah  $\text{LiNi}_x\text{Co}_y\text{Mn}_z\text{O}_2$  large format lithium ion batteries has been built in this paper. The TR propagation model consists of 6 fully-charged single batteries connected through thermal resistances and can fit experiment data well. The modeling analysis focuses on discussing the influences on the TR propagation process caused by changes in different critical modeling parameters. The modeling analysis suggests possible solutions to postpone and prevent TR propagation. The simulation shows that it might be better to choose proper parameters that help prevent TR propagation rather than just postpone it, because a delay in the TR propagation process leads to a higher level of heat gathering which may cause severer thermal hazards. To prevent TR propagation, the model provides some substantial quantified solutions: (1) raise the TR triggering temperature to higher than 469 °C; (2) reduce the total electric energy released during massive internal short circuit to 75% or less of its original value; (3) enhance the heat dissipation by increasing the heat dissipation coefficient to higher than  $70 \text{ W m}^{-2} \text{ K}^{-1}$ ; (4) add extra thermal resistant layers between adjacent batteries with a thickness of 1 mm and a thermal conductivity less than  $0.2 \text{ W m}^{-1} \text{ K}^{-1}$ . One implementation, which is verified by experiment, is to insert thermal resistant layer between adjacent batteries to prevent TR propagation in the battery module.

© 2015 Elsevier Ltd. All rights reserved.

## 1. Introduction

Lithium ion battery obtains worldwide focus as a promising choice to power electric powertrains, considering its high energy density and extended cycle life [1–3]. Due to the wide range of

operating conditions, the safety issues of lithium ion batteries, especially those associated with thermal runaway (TR), have received much attention [4–6].

To diminish the possibilities of field failures, lithium ion battery has to pass test standards, i.e. UN 38.3 [7], UN R100 [8], SAE-J2464 [9], IEC-62133 [10,11], QCT-743 [12,13] and others [14–20]. In practice, however, the abuse conditions can be tricky and unpredictable [21]. Field failure cannot be eliminated and accidents happened one after another [22–28], although the batteries may have

\* Corresponding author. Tel.: +86 10 62773437; fax: +86 10 62785708.

E-mail addresses: fxx07@mails.tsinghua.edu.cn (X. Feng), ouymg@tsinghua.edu.cn (M. Ouyang).

## Nomenclature

### Variables

$A$	the surface area of the battery ( $\text{m}^2$ )
$A_{j,y}$	the area in direction $j$ of node $y$ for heat flow to pass ( $\text{m}^2$ )
$A_x$	the frequency factor for the reaction with reactant $x$ ( $\text{s}^{-1}$ )
$C_p$	the specific heat capacity ( $\text{J kg}^{-1} \text{K}^{-1}$ )
$c_x$	the normalized concentration of reactant $x$ (1)
$c_{x,0}$	the initial value of $c_x$ in the model (1)
$c_{\text{SEI},0}^{\text{ref}}$	the reference concentration for the SEI regeneration reaction (1)
$\frac{dt}{dt}$	the derivative of the temperature ( $\text{K s}^{-1}$ )
$\frac{dc_x}{dt}$	the derivative of $c_x$ ( $\text{s}^{-1}$ )
$E_{a,x}$	the activation energy of the Arrhenius Equation for reactant $x$ ( $\text{J mol}^{-1}$ )
$g_x$	the correction term of the Arrhenius Equation for reactant $x$ (1)
$h_{\text{dis}}$	the average heat dissipation coefficient ( $\text{W m}^{-2} \text{K}^{-1}$ )
$K_{\text{SEI}}^g$	the proportion factor for the SEI regeneration reaction (1)
$M$	the mass (g, kg)
$m_x$	the mass of reactant $x$ (g)
$n_{x,1}, n_{x,2}$	the orders of the Arrhenius Equation for the reaction with reactant $x$ (1)
$Q$	the heat generation/transfer power (W)
$R$	the ideal gas constant, $R = 8.314 \text{ J mol}^{-1} \text{ K}^{-1}$ ( $\text{J mol}^{-1} \text{ K}^{-1}$ )
$R_{j,y}$	the thermal resistance toward direction $j$ for node $y$ ( $\text{m}^2 \text{ K W}^{-1}$ )
$R_z$	the thermal resistance toward direction $j$ for component $z$ ( $\text{m}^2 \text{ K W}^{-1}$ )
$T$	the temperature. Use Kelvin as its unit in Arrhenius Equations ( $^\circ\text{C}$ , K)
$T_{\text{amb}}$	the ambient temperature ( $^\circ\text{C}$ )
$T_{i,i+1}$	the temperature between Bat $i$ and Bat $i + 1$ ( $^\circ\text{C}$ )
$T_{\text{onset},x}$	the onset temperature for the reaction with reactant $x$ ( $^\circ\text{C}$ )

$T_{\text{TR,ARC}}$	the triggering temperature of TR determined by ARC test ( $^\circ\text{C}$ )
$t$	the time (s)
$\Delta H$	the energy released during TR (J)
$\Delta T$	the total temperature rise during TR ( $^\circ\text{C}$ , K)
$\Delta t$	the average time for the internal short circuit during TR (s)
$\delta_\Delta$	the thickness of the thermal resistant layer (m)
$\lambda_\Delta$	the heat conductivity for the thermal resistant layer ( $\text{W m}^{-1} \text{ K}^{-1}$ )

### Subscripts

$b$	denotes that the variable is for the back cell within the battery
$e$	denotes that the power $Q$ is generated by internal short circuit
$f$	denotes that the variable is for the front cell within the battery
$h$	denotes that the power $Q$ is for the heat transfer/dissipation into the neighbors/environment
$i$	denotes that the variable is for the Bat $i$
$j$	denotes that the variable is for the heat transfer toward direction $j$ , as in Fig. 4
$r$	denotes that the power $Q$ is generated by chemical reactions
$x$	denotes that the variable is for reactant $x$ , as listed in Table 2
$y$	denotes that the variable is for node $y$ , as listed in Table 4
$z$	denotes that the thermal resistance is for component $z$ , as listed in Table 9

### Superscripts

$d$	the decomposition of the reactant
$g$	the regeneration of the reactant

passed the respective test standards. Initiations of battery safety problems cannot be fully considered in the test standards until it occurs in field applications. For example, the loose contact of connectors [23], unpredictable crush and electrolyte leakage [24], and internal short circuit during operation [27,28] are some of the abuse conditions that was not included in the test standards but arouse battery safety problems.

Once the TR of a single cell is triggered, TR propagation to neighboring cells can lead to catastrophic hazards [27–29]. Therefore prevention of TR propagation must be considered in battery pack design [30]. We may need massive experiments on TR propagation to help design a safe battery pack, although few current literature provide experimental data related on TR propagation but [31] to the best knowledge of the authors. However, since experimental study on TR propagation within a battery pack costs much time and money, building an easy-to-use, verified abuse model that realistically captures TR propagation mechanisms in battery pack is beneficial to help us find efficient approaches to prevent TR propagation [29]. Building a TR propagation model takes two steps: (1) Build an accurate TR model for single cell; (2) Combine single cell TR models to build a pack model using heat transfer law between neighboring cells.

Dahn [32] and Spotnitz et al. [33] have developed a pervasively used TR model for single cell, which can predict the TR behavior of lithium ion battery well. Chemical kinetics equations, i.e.

Arrhenius Equations, have been employed to build such a TR model. The parameters in Arrhenius Equations can be obtained through experiments using accelerating rate calorimetry (ARC) [34–36], differential scanning calorimetry (DSC) [37–39], vent size package 2 [40,41] or C80 micro-calorimeter [42,43]. Furthermore, the single cell TR model has been applied into 3-D battery TR modeling [44,45].

TR propagation model of a battery pack consists of several single cell TR models combined together based on heat transfer law. 3-D models have been proposed and used to investigate the temperature distribution during TR propagation process, as in [30,46]. Lumped models with thermal resistance connecting different nodes as in [47] have also been proposed to investigate the TR propagation process within a battery pack [48]. However, little experimental verification for these models has been provided in literature to the best knowledge of the authors.

The goal of this paper is to build a lumped model that can predict TR propagation within a large format lithium ion battery module. TR model for single battery cell has been built and can be verified by ARC test data. The TR propagation model consists of 6 batteries connected by thermal resistance, which can also be verified by experiment data. The modeling analysis discusses the mechanisms of the TR propagation process by changing related modeling parameters. The modeling analysis suggests possible solutions to postpone and prevent TR propagation. The TR propagation is successfully prevented in the model and verified by experiment.

## 2. Overview

The model is built based on the 25 Ah lithium ion battery manufactured by AE Energy. The battery has  $\text{Li}(\text{Ni}_x\text{Co}_y\text{Mn}_z)\text{O}_2$  (NCM) cathode, graphite anode and PE-based ceramic coated separator as in [49–51]. All of the batteries were cycled about 10–20 times after delivery and then charged to full state of charge (SOC) waiting for the thermal runaway tests. The 25 Ah battery has two pouch cells inside its aluminum shell with a thickness of 1 mm, as shown in Fig. 1. The structure of the 25 Ah battery provides us a convenience to insert a micro-thermocouple between the two pouch cells to monitor the internal temperature of the battery during experiments as in [49–51]. For reference, the detailed mass proportions of the components of the 25 Ah large format lithium ion battery were reported in [50].

Table 1 provides an overview of this paper. The first column shows the definitions of cell, battery and battery module used in this paper. As the battery has such a special structure, to make a uniform definition in this paper, we define the “two pouch cells” as “cell”, the 25 Ah battery as “battery” and the 6-battery module as “battery module”. All of the batteries and cells, as listed in Table 1, are fully charged (100% State of Charge) in both modeling and experiments to represent the worst case in TR propagation.

The model structure is shown in the second column with corresponding model verification shown in the third column. The lumped cell/battery TR model is built based on Arrhenius Equations according to [32,33,44], which can be verified by the experiment using extended volume accelerating rate calorimetry (EV-ARC). The TR propagation model for the battery module is built by connecting cell TR model using heat transfer equations, which can also be verified by experiment. The TR of the first battery is triggered by penetration. Furthermore, based on the verified TR propagation model, modeling analysis for critical parameters is performed to find possible approaches to prevent TR propagation. Simulation and experimental verification have been performed for inserting thermal resistant layers between adjacent batteries to prevent TR propagation.

To present all of the contents in Table 1, this paper is organized as follows:

Section 3 presents the structure of the TR propagation model. Section 3.1 describes the lumped cell/battery TR model; Section 3.2 elucidates the TR propagation model; Section 3.3 presents the settings for TR propagation prevention in the model.

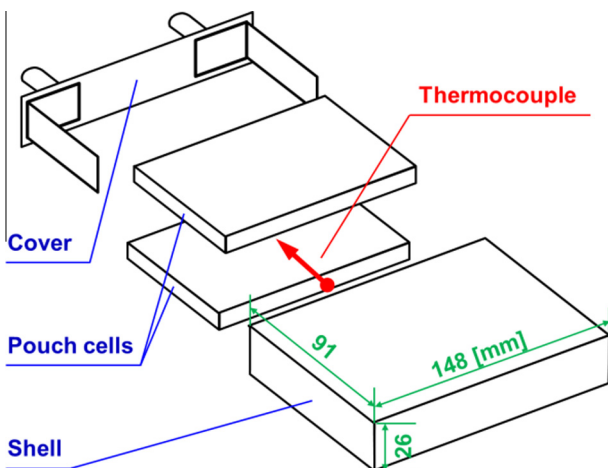


Fig. 1. The structure of the battery.

Section 4 introduces the settings of the corresponding TR experiments that are used to verify the models in Section 3. Section 4.1 describes the experiments that are used to verify the single cell/battery TR model in Section 3.1; Section 4.2 presents the TR propagation experiments that are used to verify the TR propagation model in Section 3.2; Section 4.3 introduces the TR propagation prevention tests that are used to verify the prevention method in Section 3.3.

Section 5 includes all related results and discussions on the TR propagation model. Section 5.1 provides verification of the single cell/battery model (Section 3.1) using experimental data (Section 4.1); Section 5.2 provides verification of the TR propagation model (Section 3.2) using experimental data (Section 4.2); Section 5.3 presents modeling analysis of the verified TR propagation model and discusses the influences of critical model parameters on the TR propagation process. Based on the analysis in Section 5.3, Section 5.4 discusses possible approaches that can help postpone and prevent TR propagation. The experimental verification for the prevention of TR propagation by inserting thermal resistant layers in the model is shown in Sections 5.4 and 5.4.4.

Section 6 concludes the contents and points out the prospect of this paper.

## 3. Model structure

### 3.1. TR model of the cell/battery

We assume that the cell has the same chemical kinetics as the battery considering the symmetry. Therefore the TR model in this section is both for the cell and the battery. The battery TR model is verified in Sections 4.1 and 5.1. Equivalently, the experiments in Sections 4.1 and 5.1 also verify the chemical kinetics for the cell TR model. The cell TR model is used to build the TR propagation model in Section 3.2.

In a lumped thermal model of the cell/battery, the time-variant temperature  $T(t)$  can be integrated as in Eq. (1).

$$T(t) = T(0) + \int \frac{dT(t)}{dt} dt \quad (1)$$

The derivative of  $T(t)$  satisfies Eq. (2) according to the Energy Balance, where  $M$  is the mass of the cell/battery, i.e.  $M = 720 \text{ g}$  for the battery and  $M' = M/2 = 360 \text{ g}$  for the cell;  $C_p = 1100 \text{ J/kg K}$  is the specific heat capacity of the cell/battery. Note that the battery mass  $M$  contains its accessories including shell and poles, therefore the cell mass  $M'$  also includes half of the mass of shell and poles. The specific heat capacity  $C_p$  was measured before TR test using EV-ARC, and similar values can be seen in [51,52].

$$\frac{dT(t)}{dt} = \frac{Q(t)}{MC_p} \quad (2)$$

$Q(t)$  is the total heat generation power as in Eq. (3), where  $Q_r(t)$  represents the heat generation power by chemical reactions,  $Q_e(t)$  represents the heat release power generated by massive internal short circuit during TR and  $Q_h(t)$  represents the heat transfer/dissipation power into the environment. EV-ARC can provide an adiabatic environment during test, therefore we can set  $Q_h(t) = 0$  in our cell/battery model.

$$Q(t) = Q_r(t) + Q_e(t) - Q_h(t) \quad (3)$$

**Table 1**

An overview of this paper.

Component definitions		Model	Experimental verification
<b>Cell</b>	<b>Battery</b>	$\frac{dc_x^d(t)}{dt} = A_x \cdot [c_x(t)]^{n_x} \cdot \exp(-\frac{E_{a,x}}{RT(t)})$	 
<b>Battery module</b>		$Q_{ht,y} = A_y \frac{T_y - T_{y+1}(t)}{R_y}$	
		$R_\Delta = \frac{\delta_\Delta}{\lambda_\Delta}$	

$Q_x(t)$  can be calculated by Eq. (4), where  $Q_{SEI}(t)$  denotes the heat generation power by SEI decomposition;  $Q_{anode}(t)$  denotes the heat generation power by the reaction between the intercalated Li and the solvent at anode;  $Q_{separator}(t)$  denotes the endothermic power by separator melting and thus  $Q_{separator}(t) < 0$ ;  $Q_{electrolyte}(t)$  denotes the heat generation power by the electrolyte decomposition;  $Q_{cathode}(t)$  is the heat generation power by the cathode decomposition.  $Q_{cathode}(t)$  has two terms,  $Q_{cathode,1}(t)$  and  $Q_{cathode,2}(t)$ , as shown in Eq. (5), because the NCM cathode displays two heat generation peaks in DSC tests [39,53].

$$Q_r(t) = Q_{SEI}(t) + Q_{anode}(t) + Q_{separator}(t) + Q_{electrolyte}(t) + Q_{cathode}(t) \quad (4)$$

$$Q_{cathode}(t) = Q_{cathode,1}(t) + Q_{cathode,2}(t) \quad (5)$$

The heat generation rate  $Q_x(t)$  is in proportion to the decomposition rate  $\left(\frac{dc_x^d(t)}{dt}\right)$  of the normalized concentration of reactant in reaction  $x$ ,  $c_x(t)$ , as shown in Eq. (6). The subscript  $x$  in  $Q_x(t)$  can

be SEI, anode, separator, electrolyte, cathode, 1 or cathode, 2 etc., indicating different chemical reactions.  $\Delta H_x$  is the enthalpy of the chemical reaction  $x$ ;  $m_x$  is the total mass of the reactants inside a battery;  $T_{onset,x}$  is the onset temperature of the reaction  $x$ . The determinant condition,  $T(t) > T_{onset,x}$  in the bracket means that reaction  $x$  only happens when the temperature of the cell/battery is higher than  $T_{onset,x}$ .

$$Q_x(t) = \Delta H_x \cdot m_x \cdot \frac{dc_x^d(t)}{dt}, (T(t) > T_{onset,x}) \quad (6)$$

The normalized concentration of the reactant  $x$ ,  $c_x(t)$ , can be integrated from its derivative  $\frac{dc_x(t)}{dt}$ , as shown in Eq. (7), where  $c_{x,0}$  represents the initial value of  $c_x(t)$ .  $\frac{dc_x(t)}{dt}$  equals the difference of the decomposition rate  $\frac{dc_x^d(t)}{dt}$  and the regeneration rate  $\frac{dc_x^g(t)}{dt}$  of reactant  $x$ , as shown in Eq. (8).

$$c_x(t) = c_{x,0} - \int_0^t \frac{dc_x(\tau)}{d\tau} d\tau \quad (7)$$

$$\frac{dc_x(t)}{dt} = \frac{dc_x^d(t)}{dt} - \frac{dc_x^g(t)}{dt} \quad (8)$$

The decomposition rate  $\frac{dc_x^d(t)}{dt}$  conforms with Arrhenius Equation as shown in Eq. (9), where  $A_x$  is the frequency factor;  $n_{x,1}$  and  $n_{x,2}$  are the orders for reaction  $x$ ;  $E_{a,x}$  is the activation energy;  $R = 8.314 \text{ J/(mol K)}$  is the ideal gas constant;  $g_x(t)$  is the correction term of the reaction.

$$\frac{dc_x^d(t)}{dt} = A_x \cdot [c_x(t)]^{n_{x,1}} \cdot [1 - c_x(t)]^{n_{x,2}} \cdot \exp\left(-\frac{E_{a,x}}{RT(t)}\right) \cdot g_x(t), (T(t) > T_{onset,x}) \quad (9)$$

The values of the parameters that are related to chemical kinetics and have  $x$  as subscripts have been listed in Table 2. For the SEI decomposition shown in Table 2,  $x = \text{SEI}$ ,  $n_{x,1} = 1$ ,  $n_{x,2} = 0$  and  $g_x(t) = 1$ , so we can get Eq. (10).

$$\frac{dc_{\text{SEI}}^d(t)}{dt} = A_{\text{SEI}} \cdot c_{\text{SEI}}(t) \cdot \exp\left(-\frac{E_{a,\text{SEI}}}{RT(t)}\right), (T(t) > T_{onset,\text{SEI}}) \quad (10)$$

SEI can be regenerated due to Li-solvent reaction at the anode [34,54], such a regeneration can balance out the SEI decomposition. Therefore, the derivative of  $c_{\text{SEI}}(t)$  is the difference of the SEI decomposition rate and regeneration rate as shown in Eq. (11).

$$\frac{dc_{\text{SEI}}(t)}{dt} = \frac{dc_{\text{SEI}}^d(t)}{dt} - \frac{dc_{\text{SEI}}^g(t)}{dt} \quad (11)$$

Let the SEI regeneration rate  $\frac{dc_{\text{SEI}}^g(t)}{dt}$  be proportional to the reaction rate of Li-solvent reaction, as shown in Eq. (12), where  $K_{\text{SEI}}^g = 5$  is the proportion factor to fit the experimental data.

$$\frac{dc_{\text{SEI}}^g(t)}{dt} = K_{\text{SEI}}^g \cdot \frac{dc_{\text{anode}}^d(t)}{dt} \quad (12)$$

For the Li-solvent reaction at anode we have Eq. (13), where  $x = \text{anode}$ ,  $n_{x,1} = 1$ ,  $n_{x,2} = 0$  and the correction term  $g_{\text{anode}}(t) = \exp\left(-\frac{c_{\text{SEI}}(t)}{c_{\text{SEI},0}^{\text{ref}}}\right)$ , and  $c_{\text{SEI},0}^{\text{ref}} = 1$ .

$$\begin{aligned} \frac{dc_{\text{anode}}^d(t)}{dt} &= A_{\text{anode}} \cdot c_{\text{anode}}(t) \\ &\cdot \exp\left(-\frac{E_{a,\text{anode}}}{RT(t)}\right) \cdot \exp\left(-\frac{c_{\text{SEI}}(t)}{c_{\text{SEI},0}^{\text{ref}}}\right), (T(t) > T_{onset,\text{anode}}) \end{aligned} \quad (13)$$

$Q_e(t)$  in Eq. (3) represents the heat generation rate for massive internal short circuit that happens when the separator collapses at TR.  $Q_e(t)$  can be calculated by Eq. (14), where  $\Delta H_e$  is the total electrical energy released to heat the battery during massive internal short circuit;  $\Delta t$  is the average short circuit time when TR happens, here  $\Delta t = 10 \text{ s}$  for the cell/battery TR model;  $T_{TR,ARC} = 260 \text{ }^\circ\text{C}$  is the triggering temperature of TR, because the battery used in the experiment has a PE-based ceramic coated separator with a collapse temperature of  $260 \text{ }^\circ\text{C}$  as reported in [49]. Fig. 2 illustrates the definition of  $T_{TR,ARC}$ . Fig. 2(a) is the  $T-t$  curve, whereas Fig. 2(b) is the  $dT-T$  curve for the EV-ARC test reported in [49].

$$Q_e(t) = \frac{1}{\Delta t} (\Delta H_e - \int_0^t Q_e(\tau) d\tau), (T(t) > T_{TR,ARC}) \quad (14)$$

The total energy released during TR process,  $\Delta H$ , satisfies the energy balance Eq. (15), where  $\Delta T$  represents the total temperature rise caused by self-heating of the battery during EV-ARC test;  $\Delta H_r$  is the total energy released by all of the chemical reactions, which could be calculated by Eq. (16). Different TR cases can result in different values of  $\Delta T$ , while  $\Delta H_r$  is fixed in the model. Therefore  $\Delta H_e$  has to be adjusted to fit the maximum temperature during TR in different cases.

$$\Delta H = MC_p \Delta T = \Delta H_r + \Delta H_e \quad (15)$$

$$\Delta H_r = \sum_x (c_{x,0} \cdot \Delta H_x \cdot m_x) \quad (16)$$

The first battery (including the two cells inside) is penetrated into TR, as described in Table 1. A simplified lumped penetration model for the two cells inside the first battery can be built by adding the convective cooling as Eq. (17) and changing the expression of Eq. (14) into Eq. (18) in the TR model. In a penetration model, the term of heat dissipation,  $Q_h(t)$  should be considered, as shown in Eq. (17), where  $h_{dis} = 25 \text{ W/m}^2 \text{ K}$  is the average heat dissipation coefficient, denoting the forced convective cooling inside the experiment room;  $A = 0.04 \text{ m}^2$  is the surface area of the battery;  $T(t)$  is the battery temperature, while  $T_{amb}(t) = 25 \text{ }^\circ\text{C}$  is the ambient temperature.

$$Q_h(t) = h_{dis} \cdot A \cdot (T(t) - T_{amb}(t)) \quad (17)$$

$Q_e(t)$  changes into Eq. (18) in the penetration model with a determinant condition of  $t > 0 \text{ s}$  instead of  $T > T_{TR,ARC}$ , because the massive short circuit happens at 0 s when the battery is penetrated.

**Table 2**  
Parameters used in TR model of cell/battery.

$x$	$\Delta H_x/\text{J g}^{-1}$	$m_x/\text{g}^a$	$c_{x,0}$	$n_{x,1}$ [44]	$n_{x,2}$ [44]
SEI	257 [44]	100.58	0.15 [44]	1	0
Anode	1714 [44]	100.58	1	1	0
Separator	-233.2 [44]	17.6	1	1	0
Cathode, 1	77 [39]	179.12	0.999	1	1
Cathode, 2	84 [39]	179.12	0.999	1	1
Electrolyte	800 <sup>b</sup>	108	1 [44]	1	0
$x$	$T_{onset,x}/^\circ\text{C}$	$A_x/\text{s}^{-1}$	$E_{a,x}/\text{J mol}^{-1}$	$\frac{dc_x^g(t)}{dt}$	$g_x(t)$
SEI	50	$1.667 \times 10^{15}$ [44]	$1.3508 \times 10^5$ [44]	$K_{\text{SEI}}^g \cdot \frac{dc_{\text{anode}}^d}{dt}$	1
Anode	50	$0.035 (T < 260) 5 (T > 260)$	$3.3 \times 10^4$	0	$\exp\left(-\frac{c_{\text{SEI}}(t)}{c_{\text{SEI},0}^{\text{ref}}}\right)$ [44]
Separator	120 [49]	$1.5 \times 10^{50}$	$4.2 \times 10^5$	0	1
Cathode, 1	180 [39]	$1.75 \times 10^9$ [39]	$1.1495 \times 10^5$ [39]	0	1
Cathode, 2	220 [39]	$1.077 \times 10^{12}$ [39]	$1.5888 \times 10^5$ [39]	0	1
Electrolyte	140	$3 \times 10^{15}$	$1.7 \times 10^5$	0	1

<sup>a</sup> The mass of the reactants are calculated based on the components of the 25 Ah battery [50].

<sup>b</sup> The parameters that have no citations are evaluated within practical ranges to fit the experimental data.

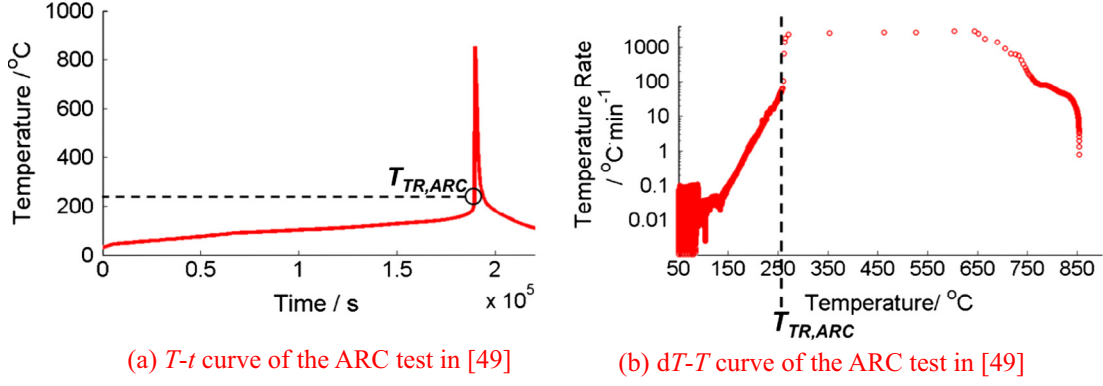
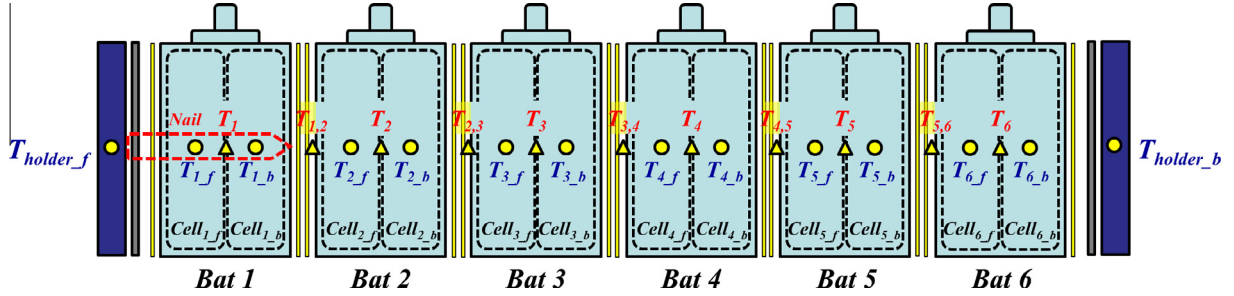
Fig. 2. The definition of  $T_{TR,ARC}$ , figures come from [49].

Fig. 3. The battery module for TR propagation model.

$$Q_e(t) = \frac{1}{\Delta t} \left( \Delta H_e - \int_0^t Q_e(\tau) d\tau \right), (t > 0 \text{ s}) \quad (18)$$

### 3.2. TR propagation model for the battery module

Fig. 3 shows the 6-battery module for TR propagation analysis. 6 batteries are clamped between 2 steel holders. The gray slices denotes the thermal resistant layers that separates the battery and the holder to avoid excessive heat leakage during experiment, whereas the yellow slices denotes the Kapton film that is used to wrap the battery to avoid short circuit through the shell during experiment. The 1st battery (Bat 1) is penetrated at its center into TR (the red dotted block in Fig. 3 shows the nail position), while the other batteries (Bat 2–Bat 6) are heated into TR due to heat propagation. The module model has 14 lumped thermal nodes: 2 of them are the holders, while the other 12 basic nodes denote the cells defined in Table 1.

Each node is assigned with a subscript  $y$  to simplify the description of the model structure, as listed in Table 3. The index  $i$  in Table 3 denotes the parameter for the  $i$ th battery (Bat  $i$ ). The relative positions for Bat  $i$  ( $i \in \{1, 2, 3, 4, 5, 6\}$ ) are shown in Fig. 3. The index  $f$  denotes “front”, which is the direction where the nail

comes in, while  $b$  denotes the inverse direction of  $f$ . Bat  $i$  has two cells inside, which are called  $Cell_{i,f}$  and  $Cell_{i,b}$  ( $i \in \{1, 2, 3, 4, 5, 6\}$ ) as shown in Fig. 3 and Table 3.

According to Eqs. (2) and (19) shows the energy balance for node  $y$ , where  $T_y(t)$  is the temperature of node  $y$ .  $M_y$  and  $C_{py}$  are the mass and the specific heat capacity of node  $y$ , respectively, with their values listed in Table 3.  $Q_y(t)$  is the heat generation power of node  $y$ , which is calculated by Eq. (20) referring to Eq. (3).

$$\frac{dT_y(t)}{dt} = \frac{Q_y(t)}{M_y C_{py}} \quad (19)$$

$$Q_y(t) = Q_{r,y}(t) + Q_{e,y}(t) - Q_{h,y}(t) \quad (20)$$

$Q_{r,y}(t)$ ,  $Q_{e,y}(t)$  and  $Q_{h,y}(t)$  in Eq. (20) refer to  $Q_r(t)$ ,  $Q_e(t)$  and  $Q_h(t)$  as in Eq. (3), respectively. Corresponding equations to calculate the terms in Eq. (20) are listed in Table 4.  $Q_{r,y}(t) = Q_{e,y}(t) = 0$  for the holders, which do not generate heat.  $Q_{r,y}(t) = Q_r(t)$  for the cells according to Eq. (4). Note that when calculating  $Q_{r,y}(t)$ ,  $T(t)$  should be substituted by  $T_y(t)$ , which is the temperature of node  $y$ .

Each cell has 6 directions of heat dissipation, as shown in Fig. 4. Therefore  $Q_{h,y}(t)$  satisfies Eq. (21), where  $Q_{1h,y}$ ,  $Q_{2h,y}$ ,  $Q_{3h,y}$ ,  $Q_{4h,y}$ ,  $Q_{5h,y}$  and  $Q_{6h,y}$  represent the heat transfer power to the front, back, left, right, up and down side for node  $y$ , respectively.  $T_{y-1}$  ( $T_{y+1}$ )

Table 3

The values for subscript  $y$  for different nodes.

$y$	Description	$M_y/\text{kg}$	$C_{py}/\text{J kg}^{-1} \text{K}^{-1}$
$i,f, i \in \{1, 2, 3, 4, 5, 6\}$	The front (toward the nail) half battery including the front cell	0.36	1100
$i,b, i \in \{1, 2, 3, 4, 5, 6\}$	The back half battery including the back cell	0.36	1100
$holder\_f (holder\_b)$	The front (back) holder used to clamp the battery module	0.474	460

Table 4  
The terms for Eq. (20) to calculate  $Q_y(t)$ .

$y$	$Q_{r,y}(t)$	$Q_{e,y}(t)$	$Q_{h,y}(t)$
$1,f, 1\_b$	Eq. (4)	Eq. (18)	Eq. (21)
$i,f, i \in \{2, 3, 4, 5, 6\}$	Eq. (4)	Eq. (14)	Eq. (21)
		Eq. (27)	
$i\_b, i \in \{2, 3, 4, 5, 6\}$	Eq. (4)	Eq. (14)	Eq. (21)
		Eq. (27)	
$holder\_f$	0	0	$Q_{h,holder}(t) - Q_{1h,1\_f}(t)$
$holder\_b$	0	0	$Q_{h,holder}(t) - Q_{2h,6\_b}(t)$

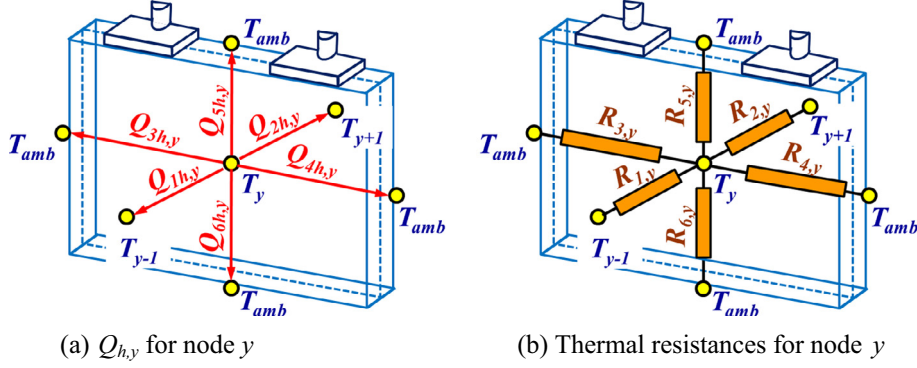


Fig. 4. Heat transfer paths for different cells.

**Table 5**  
Values of  $y - 1$  and  $y + 1$  in Fig. 4.

$y$	$y - 1$	$y + 1$
holder_f	/	1_f
holder_b	1_b	/
1_f	holder_f	1_b
$i_f, i \in \{2, 3, 4, 5, 6\}$	$i - 1_b$	$i_b$
$i_b, i \in \{1, 2, 3, 4, 5\}$	$i_f$	$i + 1_f$
6_b	6_f	holder_b

**Table 6**  
Equations for calculating  $Q_{jh,y}$ .

$j$	$Q_{jh,y}$
$j = 1$	$Q_{1h,y} = A_{1,y} \frac{T_y(t) - T_{y-1}(t)}{R_{1,y}}$ (22)
$j = 2$	$Q_{2h,y} = A_{2,y} \frac{T_y(t) - T_{y+1}(t)}{R_{2,y}}$ (23)
$j \in \{3, 4, 5, 6\}$	$Q_{jh,y} = A_{j,y} \frac{T_y(t) - T_{amb}(t)}{R_{j,y}}$ (24)

**Table 7**  
Values of areas used in the model.

$A$	Area/m <sup>2</sup>
$A_{1,y}, A_{2,y}$	0.01354
$A_{3,y}, A_{4,y}$	0.001202
$A_{5,y}, A_{6,y}$	0.001952
$A_{h,holder}$	0.05

means the temperature of the front (back) node that is connected to node  $y$ , the descriptions of which have been listed in Table 5.

$$Q_{hy}(t) = \sum_{j=1}^6 Q_{jh,y}(t) \quad (21)$$

$Q_{jh,y}$  ( $j \in \{1, 2, 3, 4, 5, 6\}$ ) can be calculated by equations as listed in Table 6, employing the method of thermal resistance circuits in heat transfer theory, as shown in Fig. 4b.  $R_{j,y}$  ( $j \in \{1, 2, 3, 4, 5, 6\}$ )

denotes the thermal resistance toward different heat transfer directions, while  $A_{j,y}$  ( $j \in \{1, 2, 3, 4, 5, 6\}$ ) denotes the corresponding area for heat flow to pass.

The  $Q_{h,holder}(t)$  listed in Table 4 means the heat dissipation to the ambient for the two holders, which can be calculated by Eq. (25), where  $T_{amb}(t)$  denotes the ambient temperature,  $T_{holder}$  represents the temperature of the holder,  $R_{h,holder}$  is the thermal resistance of heat dissipation and  $A_{h,holder}$  is the surface area of the holder.

$$Q_{h,holder}(t) = A_{h,holder} \frac{T_{holder}(t) - T_{amb}(t)}{R_{h,holder}} \quad (25)$$

The values of those areas  $A$  used in model have been listed in Table 7, based on the geometry.

$R_{j,y}$  ( $j \in \{1, 2, 3, 4, 5, 6\}$ ) denotes the total thermal resistance in direction  $j$ . The equations that are used to calculate  $R_{j,y}$  are listed in Table 8. Each  $R_{j,y}$  is a sum of many physical based thermal resistances  $R_z$ , as in Eq. (26).

$$R_{j,y} = \sum_z R_z \quad (26)$$

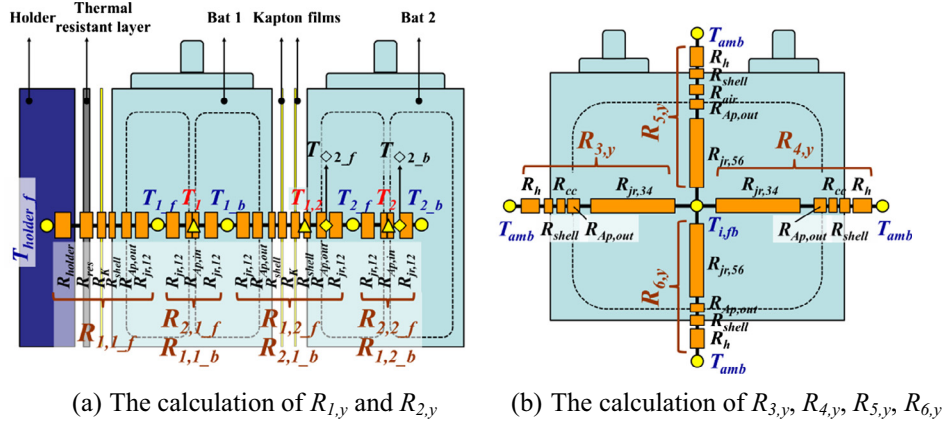
The definitions of different  $R_z$  have been shown in Fig. 5 and listed in Table 9.  $R_z$  can be the thermal resistance of the holder,  $R_{holder}$ ; or the thermal resistance of the core in the 1–2 direction,  $R_{jr,12}$  etc. Fig. 5(a) shows the relative positions of different  $R_z$  that are used to calculate  $R_{1,y}$  and  $R_{2,y}$ , while Fig. 5(b) shows the relative positions of different  $R_z$  that are used to calculate  $R_{j,y}$  ( $j \in \{3, 4, 5, 6\}$ ).

$R_z$  can be divided into 3 categories: the heat conduction resistance, the contact thermal resistance and the thermal resistance for the average heat dissipation from battery surface to the ambient. Different categories of  $R_z$  require different equations.

In a TR propagation model, the TR determinant condition in calculating  $Q_e(t)$  changes from  $T(t) \geq T_{TR,ARC}$  in Eq. (14) to  $T_{\diamond i,f}(t)$ ,  $T_{\diamond i,b}(t) \geq T_{TR,ARC}$  in Eq. (27).  $T_{\diamond i,f}(t)$  ( $T_{\diamond i,b}(t)$ ) denotes the temperature at the front edge of the core of the front (back) cell, as the yellow diamond shown in Fig. 5(a). The determinant condition changes because the Cell<sub>2,f</sub> ~ Cell<sub>6,b</sub> suffers side heating in a TR propagation test and the temperature at the front edge is the highest. Whenever the temperature at the front edge of the cell reaches

**Table 8**  
The equations for calculating  $R_{j,y}$ .

$y$	$R_{1,y}$	$R_{2,y}$	$R_{3,y} = R_{4,y}$	$R_{5,y}$	$R_{6,y}$
1_f	$R_{holder} + R_{res} + R_K + R_{shell}$ $+ R_{Ap,out} + R_{jr,12}$	$2 \times (R_{jr,12} + R_{Ap,in})$	$R_{jr,34} + R_{Ap,out} + R_{cc}$ $+ R_{shell} + R_h$	$R_{jr,56} + R_{Ap,out} + R_{air}$ $+ R_{shell} + R_h$	$R_{jr,56} + R_{Ap,out}$ $+ R_{shell} + R_h$
$i_f, i \in \{2, 3, 4, 5, 6\}$	$2 \times (R_K + R_{shell} + R_{Ap,out} + R_{jr,12})$	$2 \times (R_{jr,12} + R_{Ap,in})$			
$i_b, i \in \{1, 2, 3, 4, 5\}$	$2 \times (R_{jr,12} + R_{Ap,in})$	$2 \times (R_K + R_s + R_{Ap,out} + R_{jr,12})$			
6_b	$2 \times (R_{jr,12} + R_{Ap,in})$	$R_{holder} + R_{res} + R_K + R_s$ $+ R_{Ap,out} + R_{jr,12}$			

Fig. 5. The definition of  $R_z$  listed in Table 8 to calculate  $R_{j,y}$ .

**Table 9**  
The definition of  $R_z$  and relative specifications.

Equation	$R_z$	Definition	$\delta/m$	$\lambda/W\text{ m}^{-1}\text{ K}^{-1}$	$h/W\text{ m}^{-2}\text{ K}^{-1}$
Conduction resistance $R_z = \delta/\lambda$	$R_{holder}$	Resistance of the holder	0.01	40	/
	$R_{res}$	Resistance of the thermal resistant layer between the battery and the holder	0.0015	0.08	/
	$R_{shell}$	Resistance of the battery shell.	0.001	238	/
	$R_{jr,12}$	Resistance of the wined core toward 1 or 2 direction.	0.006	1.5	/
	$R_{jr,34}$	Resistance of the wined core toward 3 or 4 direction.	0.070	30	/
	$R_{jr,56}$	Resistance of the wined core toward 5 or 6 direction.	0.041	30	/
	$R_{air}$	Resistance of the air gap between the cell core and the battery cover.	0.005	0.0321	/
	$R_{cc}$	Resistance of the current collector	0.0025	0.25	/
Contact resistance $R_z = 1/h$	$R_K$	Equivalent resistance of the Kapton film that is used to wrap the battery in experiment.	/	/	420
	$R_{Ap,out}$	Equivalent resistance of the outside aluminum plastic film.	/	/	195
	$R_{Ap,in}$	Equivalent resistance of the inside aluminum plastic film.	/	/	1000
Heat dissipation resistance $R_z = 1/h_{dis}$	$R_h$	The average heat dissipation resistance from the battery surface to the ambient, including heat convection and radiation.	/	/	25

$T_{TR,ARC}$ , TR will happen because local collapse of the separator will lead to massive internal short circuit.

$$Q_e(t) = \frac{1}{\Delta t} (\Delta H_e - \int_0^t Q_e(\tau) d\tau), (T_{phi,i,f}(t), T_{phi,i,b}(t) \geq T_{TR,ARC}) \quad (27)$$

$T_{phi,i,f}(t)$  ( $T_{phi,i,b}(t)$ ) can be interpolated using Eq. (28) (Eq. (29)), according to the thermal resistance circuit as shown in Fig. 5(a). Note that in Fig. 5(a) we have shown  $T_{phi,i,f}(t)$  ( $T_{phi,i,b}(t)$ ) for  $i = 2$ .

$$T_{phi,i,f}(t) = T_{i,f}(t) + \frac{R_{jr,12}}{R_{1,2,f}} (T_{i-1,b}(t) - T_{i,f}(t)) \quad (28)$$

$$T_{phi,i,b}(t) = T_{i,b}(t) + \frac{R_{jr,12}}{R_{1,2,b}} (T_{i,f}(t) - T_{i,b}(t)) \quad (29)$$

### 3.3. Prevention of TR propagation in the model

Inserting a thermal resistant layer between adjacent batteries is a possible approach to inhibit TR propagation. Fig. 6 shows the battery module with thermal resistant layer (gray strips) inserted between adjacent batteries.  $R_\Delta$  in Fig. 6 represents the thermal resistance of the inserted thermal resistant layer. Suppose the thermal resistant layer has a thermal conductivity of  $\lambda_\Delta$  and a thickness of  $\delta_\Delta$ ,  $R_\Delta$  can thus be calculated by Eq. (30).

$$R_\Delta = \frac{\delta_\Delta}{\lambda_\Delta} \quad (30)$$

Thermal resistance increases from  $R_{1,i+1,f}$  ( $R_{2,i,b}$ ) to  $R'_{1,i+1,f}$  ( $R'_{2,i,b}$ ) considering the extra thermal resistance  $R_\Delta$  added between Cell<sub>i,b</sub> and Cell<sub>i+1,f</sub> as shown in Eq. (31).

$$R'_{1,i+1,f} = R'_{2,i,b} = R_{1,i+1,f} + R_\Delta = R_{2,i,b} + R_\Delta \quad (31)$$

## 4. Experimental settings for model verification

### 4.1. TR test for single battery

EV-ARC test (Fig. 7a and b) and penetration test (Fig. 7c and d) on battery have been conducted to verify the TR model and the penetration model built in Section 3.1. The internal temperature was measured using a thermo-couple inserted between the two cells, as shown in Fig. 1. The internal temperature is used to verify the behavior of  $T(t)$  simulated in the model.

### 4.2. Penetration induced TR propagation in a battery module

Penetration induced TR propagation tests on a battery module were conducted using the penetration test bench inside an explosion-proof room at the Battery Test Laboratory of China Automotive Technology and Research Center (CATARC). Six batteries were clamped together using two pieces of steel holder, as illustrated in Fig. 3. The experimental settings can be seen in Fig. 8(a). Bat 1 was penetrated by the nail, while Bat 2 was heated to TR by

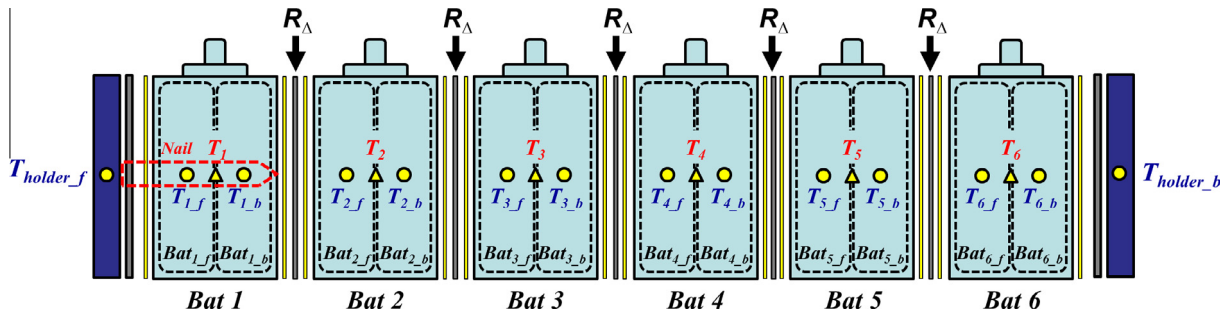
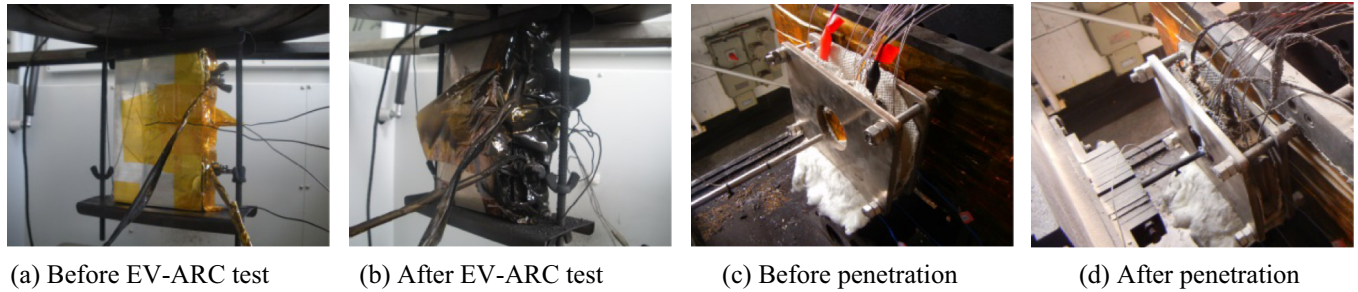


**Fig. 6.** Inserting a thermal resistant layer to prevent TR propagation.



(a) Before EV-ARC test      (b) After EV-ARC test      (c) Before penetration      (d) After penetration

**Fig. 7.** Experimental settings for verifying the TR model for cell/battery.

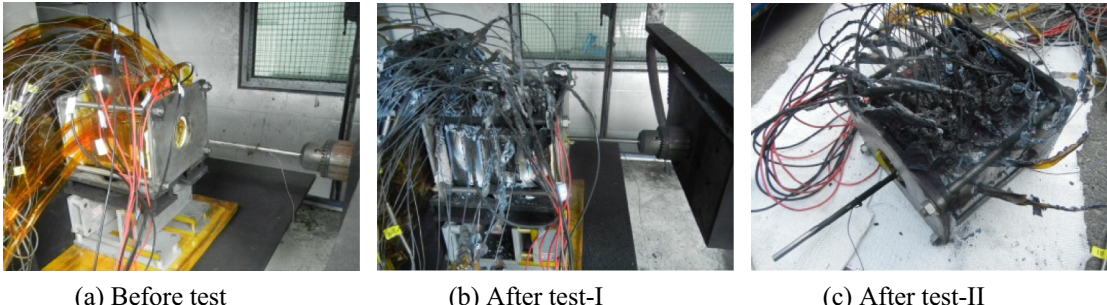


**Fig. 8.** Experimental settings for verifying the TR propagation model.

Bat 1. Kapton tape (the yellow slices in Fig. 3) of 0.6 mm thickness was used to wrap the batteries to avoid short circuits through the shell and to hold the thermocouples. Thermal resistant layers (the gray slices in Fig. 3) were inserted between the battery module and the steel holder to avoid excessive heat transfer to the holder. Fig. 8(b) and (c) illustrates the battery module after test.

Given the explosive nature of the testing, extra care had been paid to assure safety of the people and equipment involved. Cameras were employed to monitor the experiment so that the testers could stand outside the explosion-proof room to guarantee safety. An air-blower, which locates above the battery module, provides forced convective cooling during experiment.

The temperature was measured by K-type thermocouple with a sampling time of 1 s using a multi-channel data recorder TP700 manufactured by Toprie®. The placements of thermocouples are marked as yellow triangles in Figs. 3 and 5. The internal temperatures,  $T_i$  ( $i \in \{1, 2, 3, 4, 5, 6\}$ ), and the temperatures between adjacent batteries,  $T_{i,i+1}$  ( $i \in \{1, 2, 3, 4, 5\}$ ), were both measured to verify the model.

$T_i(t)$  and  $T_{i,i+1}(t)$  can both be interpolated according to the thermal resistance circuit shown in Fig. 5(a).  $T_i(t)$  is the average temperature of the two cells inside Bat  $i$  as in Eq. (32), due to

symmetry.  $T_{i,i+1}(t)$  can be interpolated by Eq. (33), where  $R_{shell}$ ,  $R_{Ap,out}$  and  $R_{jr,12}$  represent the thermal resistance of the battery shell, the outside aluminum plastic film and the jelly roll toward 1–2 direction, respectively, and relative definitions can be found in Table 9;  $R_{1,i+1,f}$  represents the total thermal resistance between Cell <sub>$i$ ,b</sub> and Cell <sub>$i+1$ ,f</sub>, which can be calculated as in Table 8.

$$T_i(t) = \frac{T_{i,f}(t) + T_{i,b}(t)}{2} \quad (32)$$

$$T_{i,i+1}(t) = T_{i,f}(t) + \frac{R_{shell} + R_{Ap,out} + R_{jr,12}}{R_{1,i+1,f}} (T_{i-1,b}(t) - T_{i,f}(t)) \quad (33)$$

#### 4.3. TR propagation prevention test

Experiment was conducted to verify the simulation results of the prevention of TR propagation as described in Section 3.3. The experimental settings can be seen in Fig. 9. Asbestos layers were inserted between adjacent batteries to block heat transfer according to Fig. 6. The asbestos layer\* has a thickness of  $\delta_{\Delta} = 1$  mm and a thermal conductivity of  $\lambda_{\Delta} = 0.07\text{--}0.1 \text{ W m}^{-1} \text{ K}^{-1}$ . The internal temperatures,  $T_i$  ( $i \in \{1, 2, 3, 4, 5, 6\}$ ), marked as yellow triangle



**Fig. 9.** Experimental settings for the prevention of TR propagation test.

inside batteries in Fig. 6, were measured by thermo-couple inserted between the two cells to verify the model.

\*The reason for the use of asbestos layers is explained in Sections 5.4 and 5.4.4.

## 5. Results and discussions

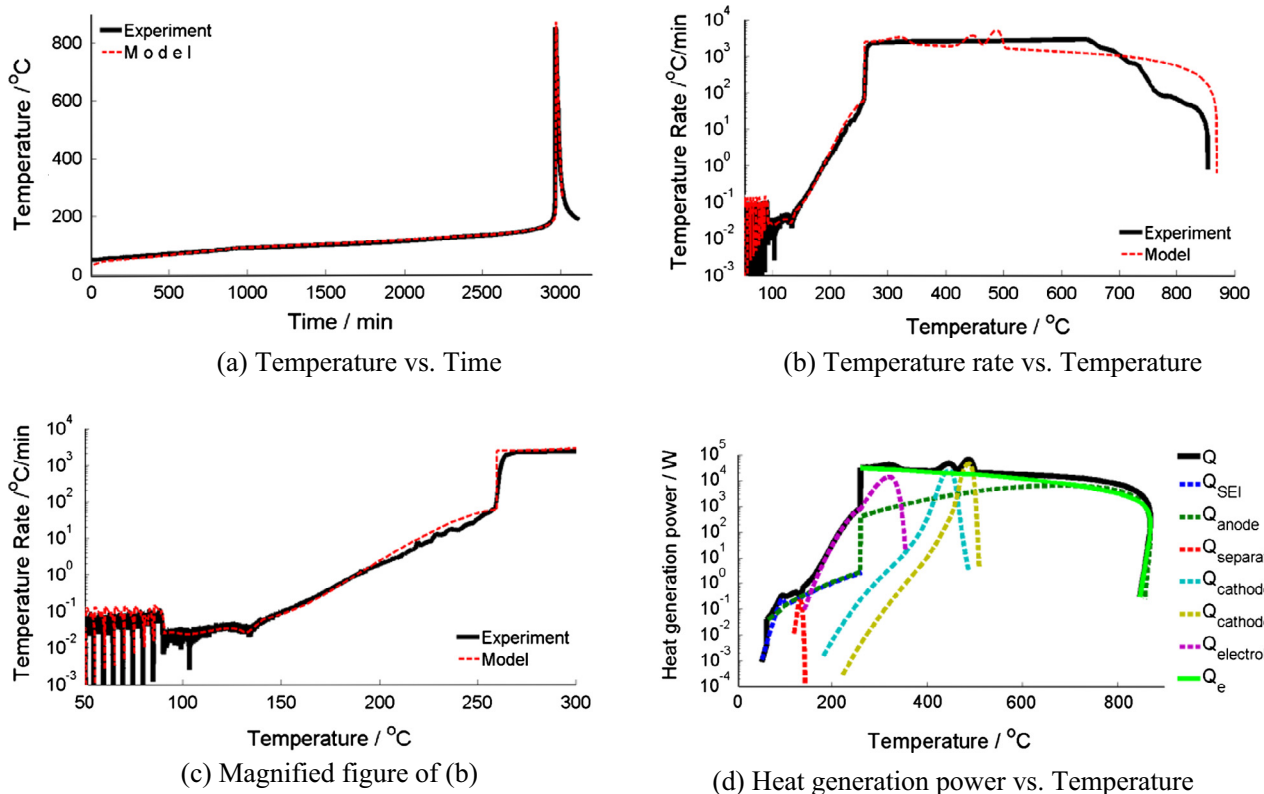
### 5.1. Experiment verification for the TR model of the cell/battery

Fig. 10 shows the model verification results for the cell TR model. The simulation results can fit the EV-ARC test results well for both the temperature-time profile and the temperature rate vs. temperature profile, as shown in Fig. 10(a–c).  $\Delta H_e = 317207 \text{ J}$  to fit the maximum temperature rise during the experiment, as in Eq. (15). Fig. 10(d) shows the heat generation power vs. temperature profile, which reveals the chemical kinetics embedded in the model.

Changing Eq. (14) into Eq. (18) to describe the internal short circuit occurred during nail penetration, the penetration model can well predict the temperature behavior during penetration, as

shown in Fig. 11. To fit the maximum temperature in the experimental result in Fig. 11(a),  $\Delta H_e = 380000 \text{ J}$  and  $\Delta t = 5 \text{ s}$  are set for Eq. (18). Fig. 11(b) shows the heat generation power vs. temperature profile, which reveals the chemical kinetics embedded in the model.

$\Delta H_e$ , representing the total electric energy released during internal short circuit, varies with different cases in the model to fit the experimental data. The release of the electric energy ( $\Delta H_e$ ) under abuse condition leads to TR of the 25 Ah battery. The 25 Ah battery has a voltage range of 2.75 V–4.2 V and a nominal voltage of 3.8 V. Therefore, the battery with 100% SOC contains about  $25 \text{ Ah} \times 3600 \text{ s} \times 3.8 \text{ V} = 342,000 \text{ J}$  electric energy. In an EV-ARC test, the test duration is long [49], and some of  $\Delta H_e$  is released due to high temperature degradation [50] before the temperature rises to  $T_{TR,ARC}$ ; however, in a penetration test, the electrical energy is released within a short period and the cut-off voltage is 0 V rather than 2.75 V. Therefore,  $\Delta H_e$  for EV-ARC test (317,207 J) is lower than the stored electric energy for a fully charged battery (342,000 J), and lower than that for penetration test (380,000 J).



**Fig. 10.** Comparison of the model simulation and the experiment for the cell TR model.

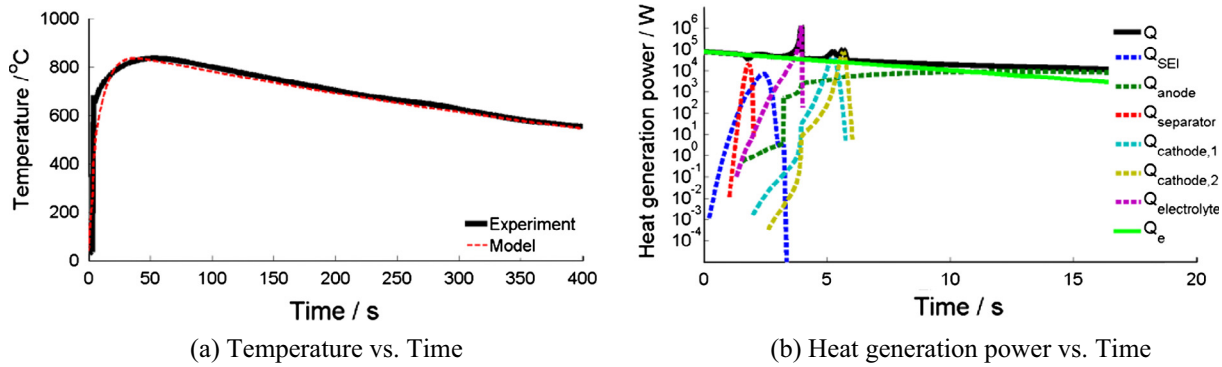


**Fig. 11.** Comparison of the model simulation and the experiment for the penetration model.

## 5.2. Experiment verification for TR propagation model

The TR propagation model described in Section 3.2 can predict TR propagation well, which is verified by the experimental data. The details of TR propagation experiments in Section 4.2 have been reported in [51], including the repetitive experiments and related discussions on temperature distribution, voltage response, fire hazard, heat transfer analysis, and material changes etc. The readers are referred to [51] for more details of the experiments.

Fig. 12 shows that both  $T_i(t)$  and  $T_{i,i+1}(t)$  calculated by Eq. (32) and (33) in the TR propagation model can fit the experimental data well, given  $\Delta H_e = 400,000 \text{ J}$  for Bat 1,  $\Delta H_e = 370,000 \text{ J}$  for Bat 2–6, and  $T_{amb} = 26^\circ\text{C}$ . The dotted lines in Fig. 12 are the model results, while the solid lines are the experimental results.  $D_{i \rightarrow i+1}$  denotes the TR propagation duration, as defined in Eq. (34), where  $t_{TR,i}$  represents the triggering time of TR for Bat  $i$ .  $D_{i \rightarrow i+1}$  for both the model and the experimental results have been compared in Table 10. Difference between the temperature profile of the model and the experiment is observed at after-TR time, because the thermal resistances of the materials have changed due to high temperature damage. The influences of materials changes have been discussed in our previous research, the reader is referred to [51] for more details. Despite the deviation in the after-TR behavior, the

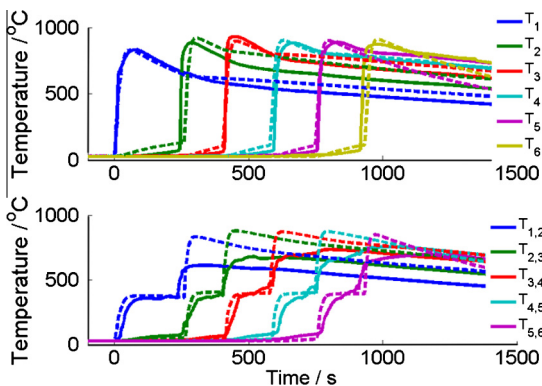


**Fig. 12.** Model verification for the TR propagation model, solid lines denotes the experimental data, dotted lines denotes the model simulation data.

advantage of the model is that it can predict the before-TR behavior of the next TR battery, which deserves more focus when doing TR propagation analysis, because we want to postpone or prevent TR propagation.

$$D_{i \rightarrow i+1} = t_{TR,i+1} - t_{TR,i}, i \in \{1, 2, 3, 4, 5\} \quad (34)$$

## 5.3. Modeling analysis of the TR propagation model

### 5.3.1. The determinant conditions of TR propagation

When TR occurs in Bat  $i$ , the temperature within Bat  $i+1$  will rise due to the side heating from Bat  $i$ . Chemical reactions as described in Eq. (9) start when the temperature within Bat  $i+1$  ( $T_{i+1,f}$  and  $T_{i+1,b}$ ) reaches corresponding  $T_{onset,x}$  as listed in Table 2. However, the heat generated by the chemical reactions is not sufficient (as shown in Fig. 10c) to heat Bat  $i+1$  into TR. It is the side heating from Bat  $i$  rather than the self-heating by the chemical reactions within Bat  $i+1$  that causes the TR propagation at Bat  $i+1$ .

According to the analysis in [51], TR propagation happens when  $T_{\diamond i,f}(t)$  ( $T_{\diamond i,b}(t)$ ), which is the temperature at the front edge of the core of Cell $_{i,f}$  (Cell $_{i,b}$ ), reaches  $T_{TR,ARC}$ , because at that time massive internal short circuit happens due to the collapse of the separator at the front edge of the cell. Fig. 13 shows the temperature profiles of  $T_{\diamond i,f}(t)$  and  $T_{\diamond i,b}(t)$  in simulation. Given the heat transfer condition set in the model,  $T_{\diamond i,f}(t)$  reaches  $T_{TR,ARC}$  slowly first, thereby follows  $T_{\diamond i,b}(t)$  to reach  $T_{TR,ARC}$  within a few seconds. However, if the thermal runaway side reactions are triggered inside the cell,  $T_{\diamond i,b}(t)$  may become higher than  $T_{\diamond i,f}(t)$  and reach  $T_{TR,ARC}$  first. Therefore the determinant condition for the TR propagation at Bat  $i$  should be Eq. (35).

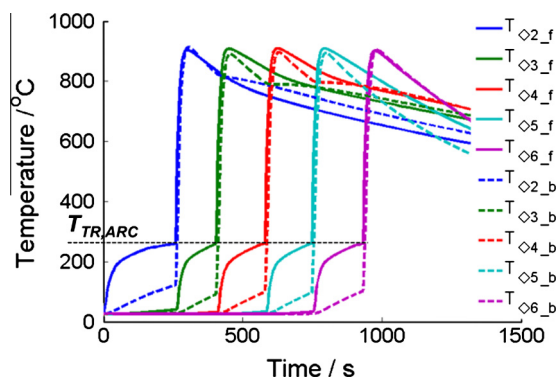


**Fig. 13.** Temperature profile of  $T_{\diamond i,f}(t)$  and  $T_{\diamond i,b}(t)$  calculated in the TR propagation model.

**Table 10**  
Comparison of the  $D_{i \rightarrow i+1}$  for the model and experiment.

Duration/s	$D_{1 \rightarrow 2}$	$D_{2 \rightarrow 3}$	$D_{3 \rightarrow 4}$	$D_{4 \rightarrow 5}$	$D_{5 \rightarrow 6}$
Experiment	245	163	186	164	159
Model	259	146	176	168	170

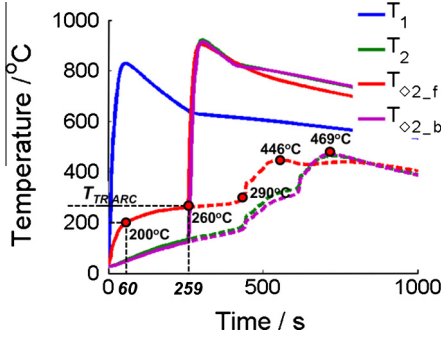


**Fig. 14.** The determinant condition of the TR propagation, solid lines are for  $T_{TR,ARC} = 260^\circ\text{C}$ , dotted lines are for  $T_{TR,ARC} = \infty$ .

$$\max\{T_{\diamond i,f}(t), T_{\diamond i,b}(t)\} \geq T_{TR,ARC}, i \in \{2, 3, 4, 5, 6\} \quad (35)$$

According to Eq. (35), TR propagation to Bat  $i$  will be prevented if Eq. (36) is satisfied. TR propagation to Bat 2 will be prevented if Eq. (37) is satisfied. Note that the prevention of TR propagation to Bat 2 means the other batteries in the whole module can survive the TR propagation hazard.

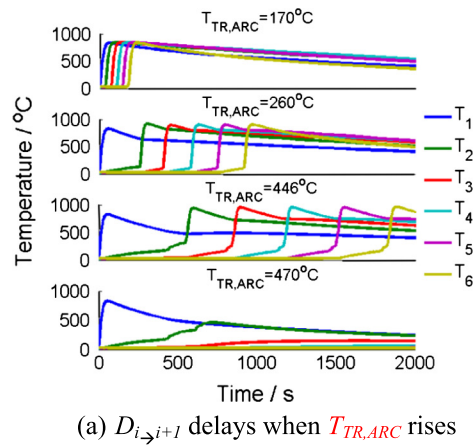
$$\max_{t \in (0, +\infty)} \{T_{\diamond i,f}(t), T_{\diamond i,b}(t)\} < T_{TR,ARC}, i \in \{2, 3, 4, 5, 6\} \quad (36)$$

$$\max_{t \in (0, +\infty)} \{T_{\diamond 2,f}(t), T_{\diamond 2,b}(t)\} < T_{TR,ARC} \quad (37)$$

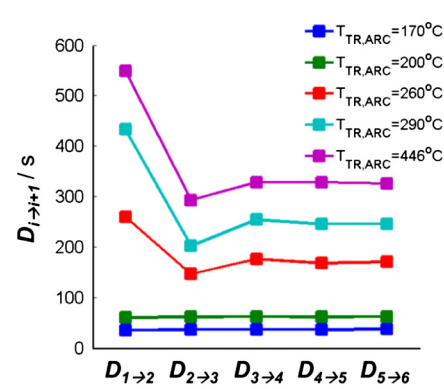
Fig. 14 shows the temperature profile of  $T_{\diamond 2,f}(t)$  and  $T_{\diamond 2,b}(t)$  during TR propagation,  $T_1(t)$  and  $T_2(t)$  are plotted for reference here. The solid lines in Fig. 14 shows that the TR at Bat 2 is triggered when  $T_{\diamond 2,f}(t)$  reaches  $T_{TR,ARC} = 260^\circ\text{C}$ . Assuming  $T_{TR,ARC} = \infty$ , or in other words, supposing that the separator is strong enough to bear extreme temperature, we can use the dotted lines to investigate the maximum temperature that  $T_{\diamond 2,f}(t)$  and  $T_{\diamond 2,b}(t)$  can reach. Before  $T_{\diamond 2,f}(t)$  reaches  $290^\circ\text{C}$ , heat transfer from Bat 1 dominates the reason of the temperature rise, while after  $T_{\diamond 2,f}(t)$  reaches  $290^\circ\text{C}$ , thermal runaway side reactions inside Cell<sub>2,f</sub> and Cell<sub>2,b</sub> are triggered to lift their temperature to a higher level.  $T_{\diamond 2,f}(t)$  reaches its maximum value of  $446^\circ\text{C}$  at 560 s, then  $T_{\diamond 2,b}(t)$  reaches its maximum value of  $469^\circ\text{C}$  at 723 s. Therefore suppose that  $T_{TR,ARC}$  is higher than  $469^\circ\text{C}$ , TR propagation will be prevented because  $T_{\diamond 2,f}(t)$  and  $T_{\diamond 2,b}(t)$  will never reach  $T_{TR,ARC}$ . When  $T_{TR,ARC}$  is less than  $469^\circ\text{C}$ , the TR propagation time ( $D_{i \rightarrow i+1}$ ) increases as  $T_{TR,ARC}$  increases. For example,  $D_{1 \rightarrow 2}$  increases from 60 s to 259 s if  $T_{TR,ARC}$  increases from  $200^\circ\text{C}$  to  $260^\circ\text{C}$ , as shown in Fig. 14.

### 5.3.2. Modeling analysis of critical parameters

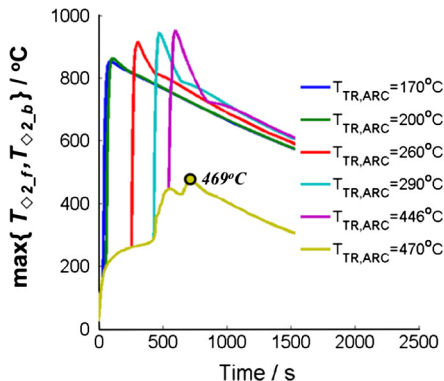
Modeling analysis has been performed on the critical parameters that may influence the TR propagation process. The results can help find solutions to prevent TR propagation within large format lithium ion battery module. To match Eq. (37) to prevent the TR propagation, we can try approaches that can either increase  $T_{TR,ARC}$  or decrease  $T_{\diamond 2,f}(t)$  and  $T_{\diamond 2,b}(t)$ . To decrease  $T_{\diamond 2,f}(t)$  and



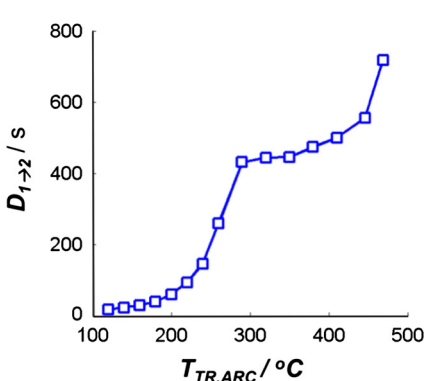
(a)  $D_{i \rightarrow i+1}$  delays when  $T_{TR,ARC}$  rises



(b) The relationship between  $D_{i \rightarrow i+1}$  and  $T_{TR,ARC}$



(c) The variation of  $\max\{T_{\diamond 2,f}(t), T_{\diamond 2,b}(t)\}$  for different  $T_{TR,ARC}$



(d) The relationship between  $D_{1 \rightarrow 2}$  and  $T_{TR,ARC}$

**Fig. 15.** The influence of  $T_{TR,ARC}$  on the TR propagation result.

$T_{\diamond 2\_b}(t)$ , we can diminish the total energy released during TR, increase the heat dissipation of the battery, or block the heat transfer between Bat 1 and Bat 2. Therefore for the modeling analysis, we can adjust four parameters: (1)  $T_{TR,ARC}$ , which denotes the triggering temperature of TR or the temperature when the separator collapses; (2)  $\Delta H_e$ , which determines the total electric energy released during TR; (3)  $h_{dis}$ , which reflects the average heat dissipation level; (4)  $R_{1,y}$  and  $R_{2,y}$ , which are the thermal resistances between adjacent batteries.

(i)  $T_{TR,ARC}$

$T_{TR,ARC}$  denotes the triggering temperature of TR, which can be determined by ARC test as in [49]. Fig. 15 illustrates the influence of  $T_{TR,ARC}$  on the TR propagation process. The TR propagation is delayed when  $T_{TR,ARC}$  increases, as shown in Fig. 15(a). The time delay of TR propagation for different batteries is shown in Fig. 15(b). Fig. 15(c) shows the temperature profile of the higher value of  $T_{\diamond 2\_f}(t)$  and  $T_{\diamond 2\_b}(t)$  in simulation with different  $T_{TR,ARC}$ . TR propagation will be prevented when  $T_{TR,ARC} = 470^\circ\text{C} > 469^\circ\text{C}$ , which is the highest temperature that front edges of the cells inside Bat 2 can reach according to Fig. 14.  $D_{1 \rightarrow 2}$ , which denotes

the TR propagation duration, increases as  $T_{TR,ARC}$  rises in simulation, as shown in Fig. 15(d).

(ii)  $\Delta H_e$

$\Delta H_e$  denotes the total electric energy released during massive internal short circuit when TR happens.  $\Delta H_e$ , together with  $\Delta H_r$ , as in Eq. (15), determines the maximum temperature that the battery can reach during TR. A lower temperature in Bat  $i$  leads to a lower temperature in Bat  $i+1$ . Therefore, the TR propagation from Bat 1 to Bat 2 will be delayed as  $\Delta H_e$  decreases, as shown in Fig. 16(a). Fig. 16(b) shows that, although  $D_{1 \rightarrow 2}$  has been delayed,  $D_{2 \rightarrow 3}$  displays no obvious delay, because the time delay of TR propagation extends the time of heat transfer from Bat 1 to Bat 2 resulting in a higher temperature in Bat 2. Fig. 16(c) shows the temperature profile of  $\max\{T_{\diamond 2\_f}(t), T_{\diamond 2\_b}(t)\}$  in simulation with different  $\Delta H_e$ . TR propagation will be prevented when  $\Delta H_e$  equals 75% or less of its original value.  $D_{1 \rightarrow 2}$ , which denotes the TR propagation time from Bat 1 to Bat 2, increases as  $\Delta H_e$  decreases in simulation, as shown in Fig. 16(d).

$\Delta H_e$  has positive correlations with the state of charge (SOC). Generally, the battery with higher SOC carries a larger  $\Delta H_e$  during

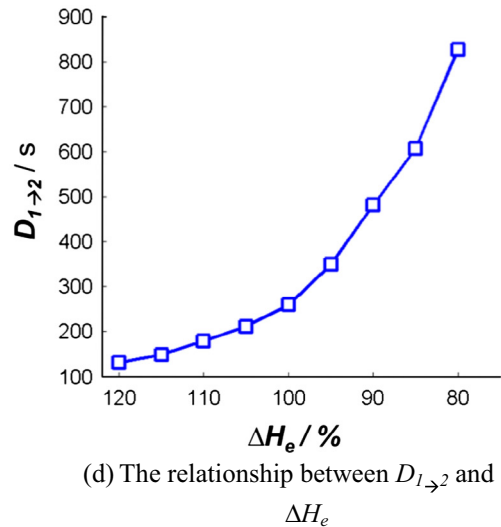
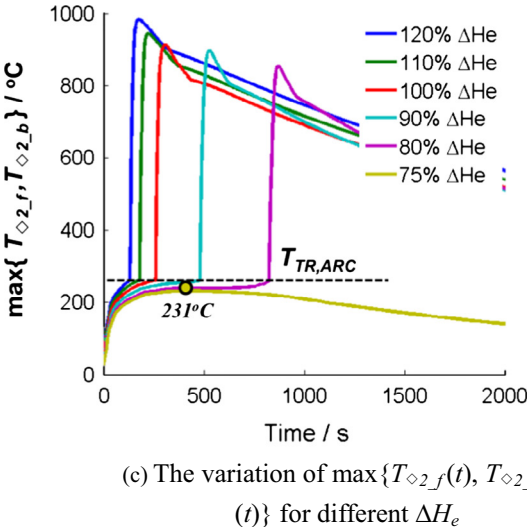
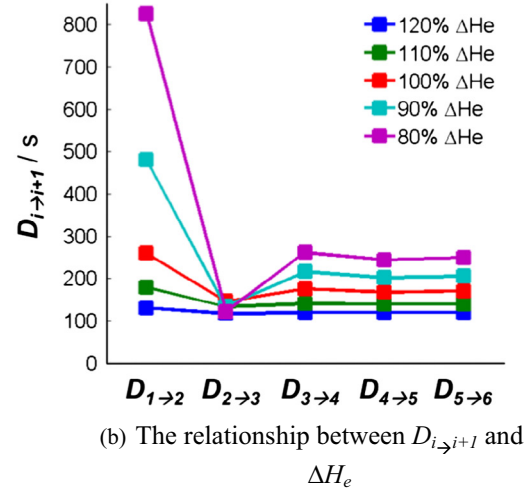
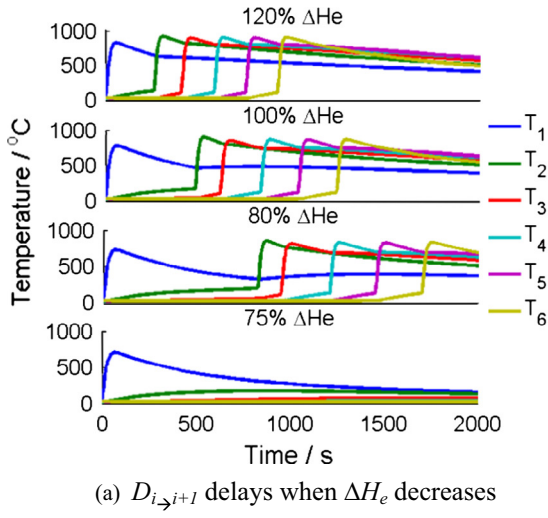
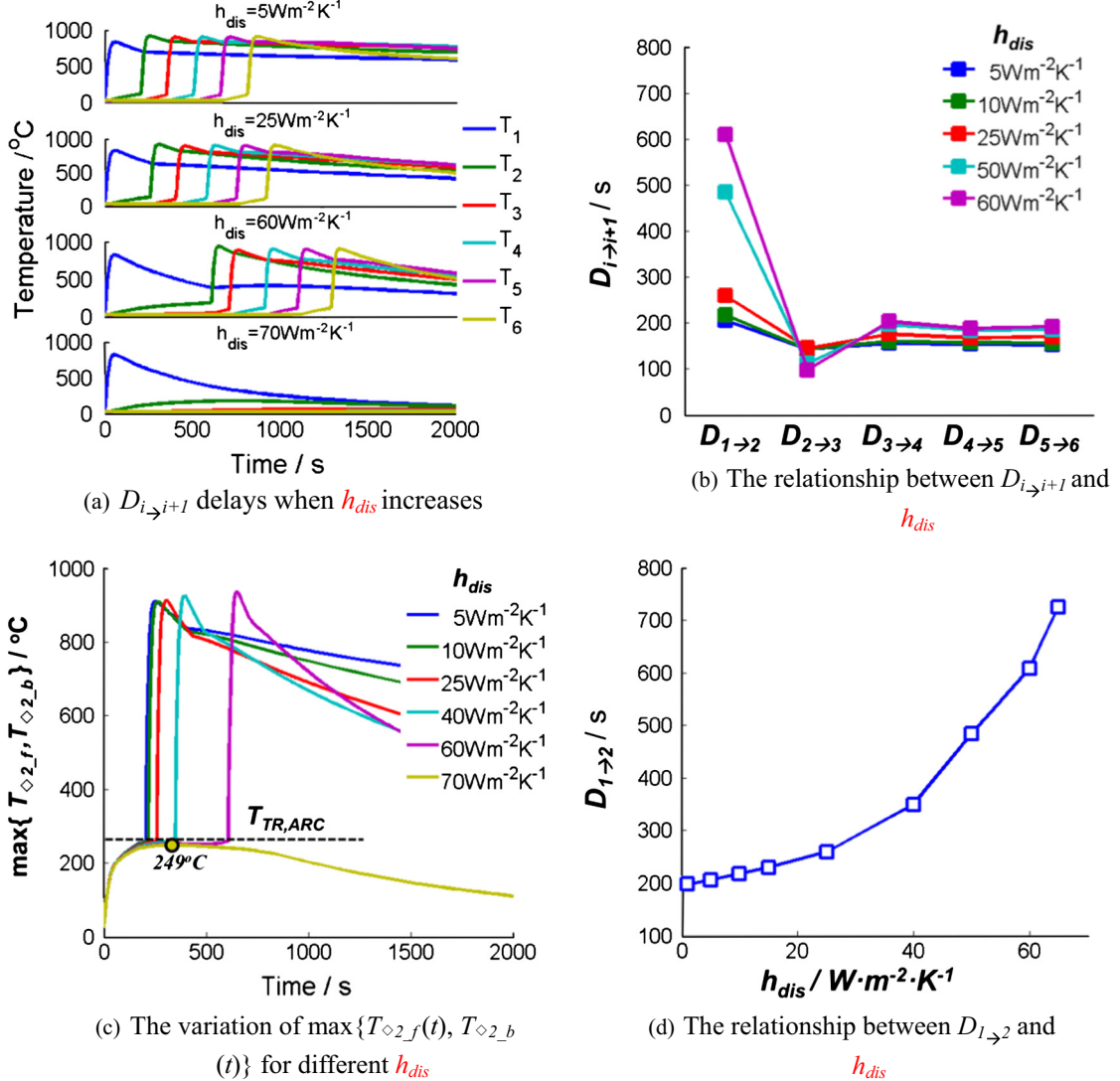


Fig. 16. The influence of  $\Delta H_e$  on the TR propagation result.

Fig. 17. The influence of  $h_{dis}$  on the TR propagation result.

TR. However, the percent of  $\Delta H_e$  does not equal to the percent of SOC, because the properties of the materials change as SOC changes.

### (iii) $h_{dis}$

$h_{dis}$  represents the average heat dissipation level surrounding the battery module. Increasing  $h_{dis}$  can lower  $\max\{T_{\diamond 2,f}(t), T_{\diamond 2,b}(t)\}$  and reduce the possibility of TR propagation from one cell to its neighbors. The TR propagation is delayed as  $h_{dis}$  increases, as shown in Fig. 17(a). The time delay of TR propagation for different batteries with different  $h_{dis}$  is shown in Fig. 17(b). The TR propagation duration  $D_{1 \rightarrow 2}$  is extended, as  $h_{dis}$  increases. However, the TR propagation time from Bat 2 to Bat 3,  $D_{2 \rightarrow 3}$ , can be always short as shown in Fig. 17(b). Bat 2 will be heated to a higher temperature due to the time extension of  $D_{1 \rightarrow 2}$ . The higher temperature of Bat 2 augments the heat propagation to Bat 3 and thus shortens  $D_{2 \rightarrow 3}$ . Fig. 17(c) shows the temperature profile of  $\max\{T_{\diamond 2,f}(t), T_{\diamond 2,b}(t)\}$  for simulation with variant  $h_{dis}$ . TR propagation will be prevented when  $h_{dis}$  is larger than  $70 \text{ W m}^{-2} \text{ K}^{-1}$ , because the  $\max\{T_{\diamond 2,f}(t), T_{\diamond 2,b}(t)\}$  can only reach  $249^\circ\text{C} < T_{TR,ARC}$ .  $D_{1 \rightarrow 2}$ , which denotes the TR propagation time from Bat 1 to Bat 2, increases as  $h_{dis}$  increases in simulation, as shown in Fig. 17(d).

### (iv) Thermal resistance $R_{1,y}$ and $R_{2,y}$

$R_{1,y}$  and  $R_{2,y}$ , the thermal resistance between adjacent batteries, is important in determining TR propagation in a battery module. Increased  $R_{1,y}$  and  $R_{2,y}$  help block the TR propagation process and allow more time for the battery to dissipate heat, thereby helping prevent TR propagation. Inserting thermal resistant layer between adjacent batteries is an applicable approach to add  $R_{1,y}$  and  $R_{2,y}$  in the design of a battery system.

Assume that we are inserting a thermal resistant layer with a thickness of  $\delta_\Delta = 1 \text{ mm}$  and a thermal conductivity of  $\lambda_\Delta$ . The added thermal resistance  $R_\Delta$  can be calculated by Eq. (30) as shown in Section 3.3. The variation of  $\lambda_\Delta$  represents the variation of  $R_\Delta$  given the fixed  $\delta_\Delta$ .

The TR propagation is postponed when  $\lambda_\Delta$  decreases, as shown in Fig. 18(a).  $\lambda_\Delta = \infty$  denotes that there is no thermal resistant layer between adjacent batteries. The delay of TR propagation time for different batteries ( $D_{i \rightarrow i+1}$ ) with variant  $\lambda_\Delta$  is shown in Fig. 18(b). The TR propagation time  $D_{1 \rightarrow 2}$  is extended as  $\lambda_\Delta$  decreases. However, the time for the TR propagation from Bat 2 to Bat 3,  $D_{2 \rightarrow 3}$ , can be shorter than  $D_{1 \rightarrow 2}$  as shown in Fig. 18(b). The extended time of the TR propagation makes Bat 2 to be heated to a higher temperature. The higher temperature of Bat 2 augments

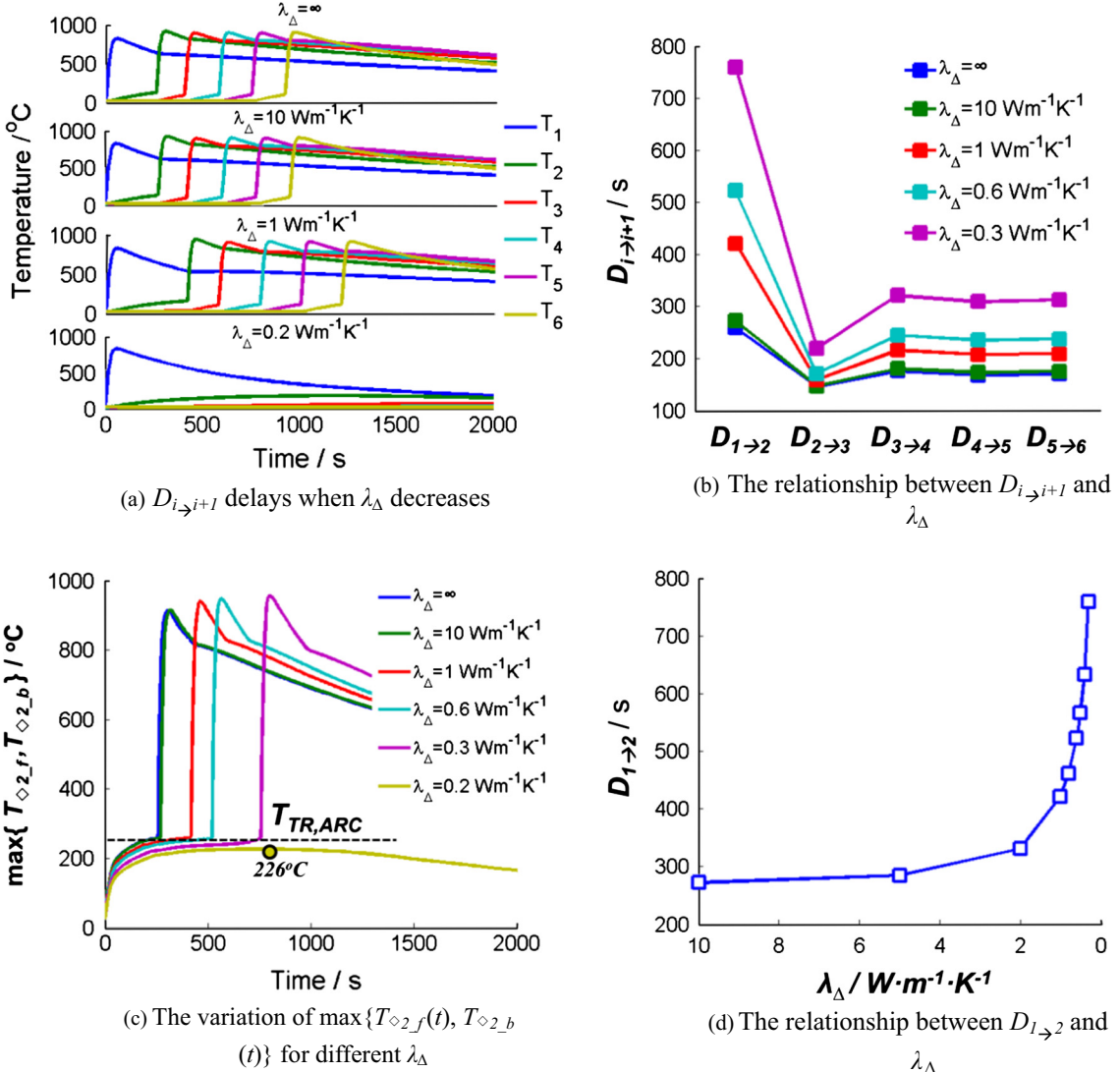


**Fig. 18.** The influence of  $\lambda_\Delta$  on the TR propagation result.

the heat propagation from Bat 2 to Bat 3 and thus shortens  $D_{2 \rightarrow 3}$ . Fig. 18(c) shows the temperature profile of  $\max\{T_{\diamond 2,f}(t), T_{\diamond 2,b}(t)\}$  in simulation with different  $\lambda_\Delta$ . TR propagation will be prevented when  $\lambda_\Delta$  equals or less than  $0.2 \text{ W m}^{-2} \text{ K}^{-1}$ , because the  $\max\{T_{\diamond 2,f}(t), T_{\diamond 2,b}(t)\}$  can only reach  $226^\circ\text{C} < T_{TR,ARC}$ .  $D_{1 \rightarrow 2}$ , which denotes the TR propagation time from Bat 1 to Bat 2, increases as  $\lambda_\Delta$  decreases in simulation, as shown in Fig. 18(d).

#### 5.4. Prevention of TR propagation within a battery module

According to the modeling analysis of the TR propagation model in Section 5.3, we can postpone and even prevent TR propagation by 4 possible approaches. A delay in TR propagation is meaningful, because it provides more time for passenger escaping and fire-fighting in case of electric vehicle crash. However, a method that can only delay TR propagation rather than prevent it may have a problem:  $D_{2 \rightarrow 3}$ , which represents the TR propagation time from Bat 2 to Bat 3, can be very short, although  $D_{1 \rightarrow 2}$  has been extended using corresponding method, as shown in the subfigures (b) of Figs. 15–18. The more time it takes for TR propagate from Bat 1 to Bat 2, the higher temperature that Bat 2 can reach during TR. And a higher temperature in Bat 2 will shorten the time for TR to propagate from Bat 2 to Bat 3. Therefore one may want to choose

proper parameters that can help prevent TR propagation rather than just propone it.

In summary, we can try to prevent TR propagation through 4 possible approaches:

##### 5.4.1. Increase the TR triggering temperature ( $T_{TR,ARC}$ ):

According to the discussion in Section 5.3.1, the TR propagation can be prevented when  $T_{TR,ARC}$  is higher than  $469^\circ\text{C}$ .  $T_{TR,ARC}$  indicates the collapse temperature of the battery separator. We can gain a higher  $T_{TR,ARC}$  by modifying the separator. As shown in Fig. 15(d), PE separator with  $T_{TR,ARC} = 130^\circ\text{C}$  [55] leads to a TR propagation time of  $D_{1 \rightarrow 2} = 21$  s, while PP separator (or PP/PE/PP composite separator) with  $T_{TR,ARC} = 170^\circ\text{C}$  [55] leads to  $D_{1 \rightarrow 2} = 35$  s. The battery we used to conduct experiment has the PE-based separator with ceramic coating as reported in [49], which will not collapse until the  $T_{TR,ARC} = 260^\circ\text{C}$ . The TR propagation time is thus extended significantly to  $D_{1 \rightarrow 2} = 259$  s. Moreover, we also find that if  $T_{TR,ARC}$  is too high ( $> 290^\circ\text{C}$ ), the thermal runaway side reactions can heat the battery temperature up internally to  $469^\circ\text{C}$ .

However, it should be noted that the discussion on preventing TR propagation through increasing the  $T_{TR,ARC}$  is based on the assumption in modeling. The increase of  $T_{TR,ARC}$  can only delay or even prevent the occurrence of internal short circuit, but not for

that of the thermal runaway side reactions. When the  $T_{TR,ARC}$  is increased to a higher level ( $>260^\circ\text{C}$  in this case), the researchers have to consider the influence of other high temperature reactions, e.g. the auto-ignition of electrolyte at  $427\text{--}465^\circ\text{C}$  as in [56] etc.

#### 5.4.2. Decrease the total electric energy released during massive internal short circuit ( $\Delta H_e$ ):

The battery pack works at different SOCs during practical operating conditions. Lower SOC denotes lower  $\Delta H_e$  that will be released during TR and thus leads to lower temperature that the battery can reach. A lower temperature makes it less possible for TR to propagate from one battery to its neighbors. TR propagation can be prevented when  $\Delta H_e$  decreases to 75% of its original value as discussed in Section 5.3.2. An implementable way to reduce  $\Delta H_e$  is to deliberately discharge the battery pack, when there is a potential of TR propagation. In this case, the adjacent batteries need to be discharged to an SOC with 75% of  $\Delta H_e$  within a specific

time  $D_{1\rightarrow 2}$  to avoid TR propagation. Another implementable way to reduce  $\Delta H_e$  is to decrease the maximum cut-off voltage during cycling, however, this leads to lower usable capacity and means lower energy density for the battery. Moreover, note that the behavior for the battery pack with full SOC, which represents the worst case in field application, is always considered when conducting safety tests.

#### 5.4.3. Improve the heat dissipation condition by increase heat dissipation coefficient ( $h_{dis}$ ):

$h_{dis}$  represents the average heat dissipation level for the battery module/pack.  $h_{dis}$  is determined by the battery module/pack design. The heat dissipation design, including the flow field design and the selection of heat transfer medium (air, water and liquid etc.), can change  $h_{dis}$  and thus influence the TR propagation process in the battery module/pack. Table 11 shows the common heat dissipation coefficients related to the heat dissipation design of a battery management system [57–60]. Based on the discussion in Section 5.3.2, the  $h_{dis}$  has to be larger than  $70 \text{ W m}^{-2} \text{ K}^{-1}$ , which requires a high speed air flow for an air cooling system. The cooling system with liquid coolant surrounding the cell, reinforced air cooling with high heat conductive plate, or heat exchange by heat pipes can easily fulfill a  $h_{dis} > 70 \text{ W m}^{-2} \text{ K}^{-1}$ . Phase change material (PCM) may also help absorb excessive TR heat through phase change [1]. However, the low thermal conductivity of PCM [61,62] may lead to insufficient heat dissipation, which needs further investigation. Another problem that should be considered is that the components in the heat dissipation design should be resistant to high temperature during TR, otherwise the heat dissipation system will be broken and thus ineffective to dissipate TR heat.

In addition, the battery pack is sometimes sealed to be waterproof. Therefore the temperature of the medium in the confined closure within the battery pack will rise sharply when TR happens at some batteries, which worsens the heat dissipation condition.

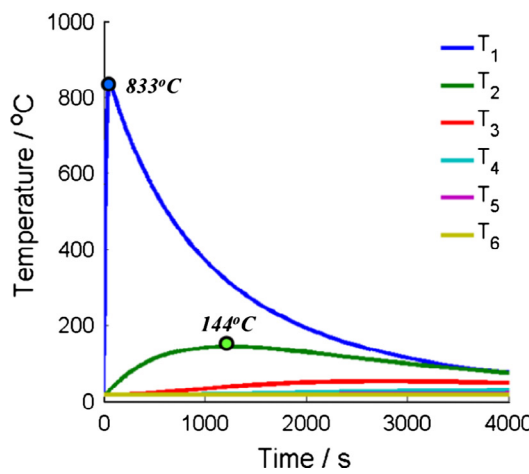
It should be noted that the “heat dissipation” we are trying to enhance here denotes the “heat dissipation to the environment” rather than the “heat dissipation to adjacent cells”. Thermal insulation, which will be discussed in the next few paragraphs, should be considered to block the heat dissipation to adjacent cells to avoid TR propagation.

**Table 11**  
Values for heat dissipation coefficients available for battery thermal management.

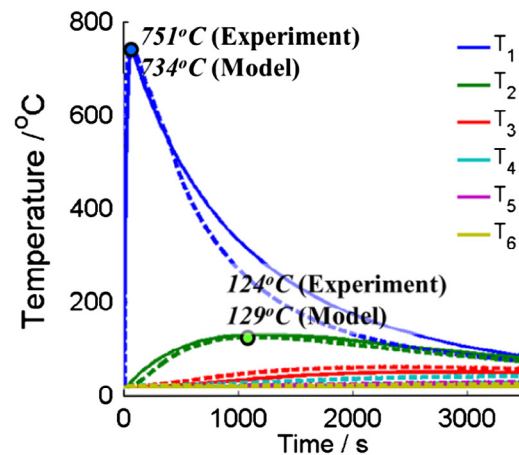
Dissipation type	$h_{dis}/\text{W m}^{-2} \text{ K}^{-1}$
Natural convection, air [57]	5–25
Forced convection, air [57]	15–250
Coolant surrounding the cell, water [58]	300–1000
Coolant surrounding the cell, oil [58]	100–700
Air cooling with aluminum plate [59]	80–90
Heat pipes, theoretical [60]	100–500

**Table 12**  
Properties for some thermal insulation materials.

Material name	Thermal conductivity/ $\text{W m}^{-1} \text{ K}^{-1}$	Maximum use temperature/°C
Perlite [63,64]	0.04–0.06 [63], 0.076 [64]	760 [63], 649 [64]
Glass fiber [63,64]	0.03–0.038	350 [63], 538 [64]
Rock wool panel [63]	0.037–0.040	800
Calcium Silicate [64]	0.065	649
Silica Aerogel [65,66]	0.02–0.09	>200 [65], 650 [66]
Asbestos [67,68]	0.07–0.1 [67]	600–1700 [68]



(a) Model prediction,  $\Delta H_e=400000\text{J}$ ,  $T_{amb}=26^\circ\text{C}$ .



(b) Model verification, the solid lines are for the model prediction ( $\Delta H_e=320000\text{J}$ ,  $T_{amb}=17^\circ\text{C}$ ) and the dotted lines are for experiment verification.

**Fig. 19.** Experimental verification for the prevention of TR propagation by inserting thermal resistant layers.

#### 5.4.4. Add extra thermal resistance between adjacent cells:

Inserting thermal resistant layer between adjacent batteries is another implementable approach to prevent TR propagation. One possible solution is to leave gaps between adjacent batteries and consider air as the thermal resistant layer. However, when TR happens, the air gap will disappear due to the battery swell. Another possible way is to insert solid thermal resistant layer between adjacent batteries, which will be discussed as follows. According to the discussion in Section 5.3.2, the inserted thermal resistant layer with a thickness of 1 mm should have a thermal conductivity of less than  $0.2 \text{ W m}^{-2} \text{ K}^{-1}$  to prevent TR propagation. We provide some thermal insulation materials that might help prevent TR propagation as in Table 12 [63–68]. In addition, note that the insulation material for TR-propagation prevention not only needs low heat conductivity, but also requires high working temperature. Here we recommend a maximum usable temperature of higher than  $500^\circ\text{C}$  according to the results in Fig. 12. Any other material with thermal conductivity lower than  $0.2 \text{ W m}^{-2} \text{ K}^{-1}$  and a maximum usable temperature higher than  $500^\circ\text{C}$  might be capable to prevent TR propagation.

However, it should be noted that thermal insulations between adjacent batteries can bring side effects. For example, the heat dissipation may get worse, the pack volume may increase, and the cost may rise. Heat dissipation and thermal insulation should be simultaneously considered during safety design. Compound layers with both high thermal conductive material and thermal resistant material [69,70] can be employed as one solution to the problem. The trade-off between the heat dissipation (discussed in Sections 5.4 and 5.4.3) and the thermal insulation (discussed in Sections 5.4 and 5.4.4) needs further investigation, and it is believed that the TR propagation in this paper can help the further investigation.

Finally, we use asbestos layer\*, the gray blocks between adjacent batteries in Fig. 6, with a thickness of  $\delta_\Delta = 1 \text{ mm}$  to separate adjacent batteries in experiment to verify the modeling analysis results.

\*Please note that asbestos layer can be carcinogenic if one is exposed to a prolonged inhalation of the asbestos fibers. However, we use asbestos layer to provide a quick example of experiment verification because it was easy to get in China. To reduce the inhalation of asbestos fibers, we have made two corresponding protective measures: (1) the asbestos layer we bought was claimed to be dust-free from the manufacturer; (2) the researchers were equipped with masks when preparing the experiments. Substitutes can be selected from Table 12 to perform future design and tests.

The asbestos layer carries a thermal conductivity of  $0.07\text{--}0.1 \text{ W m}^{-1} \text{ K}^{-1}$  according to the manufacturer. Setting  $\Delta H_e = 400000 \text{ J}$  (for Bat 1),  $T_{amb} = 26^\circ\text{C}$ ,  $\delta_\Delta = 1 \text{ mm}$  and  $\lambda_\Delta = 0.08 \text{ W m}^{-1} \text{ K}^{-1}$  in the TR propagation model according to Section 3.3, we can see that the TR propagation is prevented and the maximum temperature of Bat 2 is only  $144^\circ\text{C}$ , as shown in Fig. 19(a). The experiment verification was conducted according to Section 4.3. Bat 2 did not go through TR and TR propagation was successfully prevented in the experiment, as shown in Fig. 19(b). The maximum temperature and the ambient temperature changed in the verification experiments. Therefore, we need to adjust  $\Delta H_e = 320000 \text{ J}$  (for Bat 1) and  $T_{amb} = 17^\circ\text{C}$  to fit the experiment data. The good fit for the model and experiment, as shown in Fig. 19(b), indicates that the parameters we set for the chemical reactions and for the heat transfer are reasonable.

## 6. Conclusions

In this paper, a TR propagation model is built to guide the safety design of lithium ion battery pack. The TR propagation model consists of 6 battery models (12 cell models) connected by thermal

resistance, and can be verified by experiments. Modeling analysis of critical model parameters is used to discuss the TR propagation mechanisms. The modeling analysis helps to find solutions to prevent TR propagation.

With the help of the TR propagation model, we can obtain how much the TR propagation can be postponed or even prevented. According to the modeling analysis, a delay in the TR propagation from Bat 1 to Bat 2 may lead to a higher temperature in Bat 2, which leads to a much faster TR propagation from Bat 2 to Bat 3. Therefore one may consider proper parameters that can prevent TR propagation rather than just delay it.

The TR propagation model provides substantial quantified solutions to prevent TR propagation. And TR propagation can be prevented through 4 possible ways: (1) increase the triggering temperature ( $T_{TR,ARC}$ ) to higher than  $469^\circ\text{C}$ ; (2) decrease the total electric energy released during massive internal short circuit ( $\Delta H_e$ ) to 75% or less of its original value; (3) improve the heat dissipation condition by increase heat dissipation coefficient ( $h_{dis}$ ) to  $70 \text{ W m}^{-2} \text{ K}^{-1}$  or higher; (4) Add extra thermal resistant layers between adjacent batteries with a thickness of at least 1 mm and a thermal conductivity of less than  $0.2 \text{ W m}^{-1} \text{ K}^{-1}$ . Detailed discussions have also been provided on the implementable approaches in the practical application to prevent TR propagation.

Inserting thermal resistant layer between adjacent batteries can help prevent TR propagation. The result is predicted by the model and verified by the experiment. Future work will focus on the design of a proper battery thermal management system simultaneously considering both lower temperature inconsistency and TR propagation prevention.

## Acknowledgments

This work is funded by BMW China Services Ltd.

This work is also funded by US-China Clean Energy Research Center-Clean Vehicle Consortium (CERC-CVC), and the MOST (Ministry of Science and Technology) of China under the contract of No. 2014DFG71590. The first author appreciates the funding from China Scholarship Council. Dr. Caihao Weng (with University of Michigan, Ann Arbor) provided useful suggestions on the paper writing, appreciations should also be given to him.

## References

- [1] Ling Z, Chen J, Fang X, Zhang Z, Xu T, Gao X, et al. Experimental and numerical investigation of the application of phase change materials in a simulative power batteries thermal management system. *Appl Energy* 2014;121:104–13.
- [2] Liu R, Chen J, Xun J, Jiao K, Du Q. Numerical investigation of thermal behaviors in lithium-ion battery stack discharge. *Appl Energy* 2014;132:288–97.
- [3] Wang T, Tseng KJ, Zhao J, Wei Z. Thermal investigation of lithium-ion battery module with different cell arrangement structures and forced air-cooling strategies. *Appl Energy* 2014;134:229–38.
- [4] Larsson F, Andersson P, Blomqvist P, et al. Characteristics of lithium-ion batteries during fire tests. *J Power Sources* 2014;271:414–20.
- [5] Larsson F, Mellander B. Abuse by external heating, overcharge and short circuiting of commercial lithium-ion battery cells. *J Electrochim Soc* 2014;161(10):A1611–7.
- [6] Golubkov AW, Fuchs D, Wagner J, et al. Thermal-runaway experiments on consumer Li-ion batteries with metal-oxide and olivine-type cathodes. *RSC Adv* 2014;4:3633–42.
- [7] UN 38.3. Recommendations on the transport of dangerous goods: manual of tests and criteria. 5th revised ed. <[http://www.phmsa.dot.gov/pv\\_obj\\_cache/pv\\_obj\\_id\\_D4B2D17039E706213B36C1B309D41DCF8B4A0200/filename/UN\\_Test\\_Manual\\_Lithium\\_Battery\\_Requirements.pdf](http://www.phmsa.dot.gov/pv_obj_cache/pv_obj_id_D4B2D17039E706213B36C1B309D41DCF8B4A0200/filename/UN_Test_Manual_Lithium_Battery_Requirements.pdf)>; (accessed in 01.01.15).
- [8] UN Regulation No. 100. Uniform provisions concerning the approval of vehicles with regard to specific requirements for the electric power train, Aug. 2013. <<http://www.unece.org/fileadmin/DAM/trans/main/wp29/wp29regs/2013/R100R2e.pdf>> (accessed in 01.01.15).
- [9] SAE J2464. Electric and hybrid electric vehicle rechargeable energy storage system safety and abuse testing; 2009.
- [10] IEC-62133. Secondary cells and batteries containing alkaline or other non-acid electrolytes – safety requirements for portable sealed secondary cells, and for batteries made from them, for use in portable applications; 2002.

- [11] Cindy Millsaps. Second edition of IEC 62133: the standard for secondary cells and batteries containing alkaline or other non-acid electrolytes is in its final review cycle. *Battery power* 2012; 16(3): p. 16–8. <[http://www.nxtbook.com/nxtbooks/webcom/batterypower\\_20120506/index.php?startid=16](http://www.nxtbook.com/nxtbooks/webcom/batterypower_20120506/index.php?startid=16)>; (accessed in 01.01.15).
- [12] QCT 743. Lithium-ion batteries for electric vehicles; 2006.
- [13] QCT 743. Lithium-ion batteries for electric vehicles; 2012 (revised edition calling for opinions).
- [14] SAE J1929. Electric and hybrid vehicle propulsion battery system safety standard – lithium-based rechargeable cells; 2011.
- [15] IEC 62660-2. Secondary lithium-ion cells for the propulsion of electric road vehicles – Part 2: reliability and abuse testing; 2010.
- [16] UL 1642. Safety for lithium ion batteries; 2009.
- [17] UL 2054. Safety for household and commercial batteries; 2009.
- [18] UL 2580. Standards for batteries of use in EV; 2010.
- [19] ISO/WD 12405-2. Electrically propelled road vehicles – test specification for lithium-ion traction battery packs and systems – Part 2: high energy application; 2010.
- [20] JIS-C-8715-2. Secondary lithium cells and batteries for use in industrial applications – Part 2: tests and requirements of safety; 2012.
- [21] Ramadas P, Fang W, Zhang Z. Study of internal short in a Li-ion cell I. Test method development using infra-red imaging technique. *J Power Sources* 2014;248:769–76.
- [22] Wang Q, Ping P, Zhao X, et al. Thermal runaway caused fire and explosion of lithium ion battery. *J Power Sources* 2012;208:210–24.
- [23] Beauregard Garrett P. Report of investigation: hybrids plus plug in hybrid electric vehicle. eTec, Phoenix AZ; 2008.
- [24] Smith B. Chevrolet volt battery incident overview report. U.S. Department of Transportation, National Highway Traffic Safety Administration; 2012. p. 1.
- [25] Interim Factual Report: Boeing 787-8, JA829J Battery Fire; Case Number DCA13IA037. Washington, DC, USA: National Transportation Safety Board, Office of Aviation Safety; 2013.
- [26] Willard N, He W, Hendricks C, Pecht M. Lessons learned from the 787 Dreamliner issue on lithium-ion battery reliability. *Energies* 2013;6:4682–95.
- [27] Goto N. Aircraft serious incident investigation report: all Nippon airways Co., Ltd. JA804A. Japan Transport Safety Board, Tokyo, Japan, Rep. No. AI2014-4; September 25, 2014.
- [28] Aircraft incident report: auxiliary power unit battery fire, Japan airlines Boeing 787, JA 829J, Boston, Massachusetts, January 7, 2013. National Transportation Safety Board, DC, Rep. No. PB2014-108867; November 21, 2014.
- [29] Doughty DH. Vehicle battery safety roadmap guidance; October 2012.
- [30] Yeow KF, Teng H. Characterizing thermal runaway of lithium-ion cells in a battery system using finite element analysis approach. *SAE Int J Alt Power* 2013;2(1):179–86.
- [31] Jeevarajan JA. Hazards associated with high voltage high capacity lithium-ion batteries. *ECS Trans* 2011;33(22):1–6.
- [32] Hatchard TD, Macneil DD, Basu A, Dahn JR. Thermal model of cylindrical and prismatic lithium-ion cells. *J Electrochem Soc* 2001;148(7):755–61.
- [33] Spotnitz R, Franklin J. Abuse behavior of high-power lithium-ion cells. *J Power Sources* 2003;113:81–100.
- [34] Richard MN, Dahn JR. Accelerating rate calorimetry study on the thermal stability of lithium intercalated graphite in electrolyte: I. Experimental. *J Electrochem Soc* 1999;146(6):2068–77.
- [35] Macneil DD, Larcher D, Dahn JR. Comparison of the reactivity of various carbon electrode materials with electrolyte at elevated temperature. *J Electrochem Soc* 1999;146(10):3596–602.
- [36] Ishikawa H, Mendoza O, Sone Y, Umeda M. Study of thermal deterioration of lithium-ion secondary cell using an accelerated rate calorimeter (ARC) and AC impedance method. *J Power Sources* 2012;198:236–42.
- [37] Macneil DD, Dahn JR. Test of reaction kinetics using both differential scanning and accelerating rate calorimeters as applied to the reaction of  $\text{Li}_x\text{CoO}_2$  in non-aqueous electrolyte. *J Phys Chem: A* 2001;105:4430–9.
- [38] Roth EP, Doughty DH. Thermal abuse performance of high-power 18650 Li-ion cells. *J Power Sources* 2004;128:308–18.
- [39] Wang HY, Tang AD, Huang KL. Oxygen evolution in overcharged  $\text{Li}_{1-x}\text{Ni}_{1/3}\text{Co}_{1/3}\text{Mn}_{1/3}\text{O}_2$  electrode and its thermal analysis kinetics. *Chin J Chem* 2011;29:1583–8.
- [40] Jhu CY, Wang YW, Shu CM, et al. Thermal explosion hazards on 18650 lithium ion batteries with a VSP2 adiabatic calorimeter. *J Hazard Mater* 2011;192:99–107.
- [41] Jhu CY, Wang YW, Wen CY, Shu CM. Thermal runaway potential of  $\text{LiCoO}_2$  and  $\text{Li}(\text{Ni}_{1/3}\text{Co}_{1/3}\text{Mn}_{1/3})\text{O}_2$  batteries determined with adiabatic calorimetry methodology. *Appl Energy* 2012;100:127–31.
- [42] Wang Q, Sun J, Chen C, Zhou X. Thermal properties and kinetics study of charged  $\text{LiCoO}_2$  by TG and C80 Methods. *J Therm Anal Calorim* 2008;92(2):563–6.
- [43] Ping P, Wang Q, Huang P, Sun J, Chen C. Thermal behavior analysis of lithium-ion battery at elevated temperature using deconvolution method. *Appl Energy* 2014;129:261–73.
- [44] Kim GH, Pesaran A, Spotnitz R. A three-dimensional thermal abuse model for lithium-ion cells. *J Power Sources* 2007;170:476–89.
- [45] Guo G, Long B, Cao BG, et al. Three dimensional thermal finite element modeling of lithium-ion battery in thermal abuse application. *J Power Sources* 2010;195:2393–8.
- [46] Yang C, Kim GH, Sathanagopalan S, Pesaran A. Multi-physics modeling of thermal runaway propagation in a battery module. Meeting abstract, 223rd ECS meeting, Orlando, FL; May 2014.
- [47] Smith K, Kim GH, Darcy E, Pesaran A. Thermal/electrical modeling for abuse tolerant design of lithium ion modules. *Int J Energy Res* 2010;34:204–15.
- [48] Spotnitz R, Weaver J, Yeduvaka G, et al. Simulation of abuse tolerance of lithium-ion battery packs. *J Power Sources* 2007;163:1080–6.
- [49] Feng X, Fang M, He X, Ouyang M, Lu L, Wang H, et al. Thermal runaway features of large format prismatic lithium ion battery using extended volume accelerating rate calorimetry. *J Power Sources* 2014;255:294–301.
- [50] Feng X, Sun J, Ouyang M, He X, Lu L, Han X, et al. Characterization of large format lithium ion battery exposed to extremely high temperature. *J Power Sources* 2014;272:457–67.
- [51] Feng X, Sun J, Ouyang M, et al. Characterization of penetration induced thermal runaway propagation process within a large format lithium ion battery module. *J Power Sources* 2015;275:261–73.
- [52] Zhang J, Wu B, Li Z, Huang J. Simultaneous estimation of thermal parameters for large-format laminated lithium-ion batteries. *J Power Sources* 2014;259:106–16.
- [53] Kim H, Kong M, Kim K, et al. Effect of carbon coating on  $\text{LiNi}_{1/3}\text{Mn}_{1/3}\text{Co}_{1/3}\text{O}_2$  cathode material for lithium secondary batteries. *J Power Sources* 2007;171:917–21.
- [54] Tanaka N, Bessler WG. Numerical investigation of kinetic mechanism for runaway thermo-electrochemistry in lithium ion cells. *Solid State Ionics* 2014;262:70–3.
- [55] Arora P, Zhang Z. Battery separators. *Chem Rev* 2004;104:4419–62.
- [56] Eshetu GG, Grugnon S, Laruelle S, Boyanov S, Lecocq A, Bertrand J, et al. In-depth safety focused analysis of solvents used in electrolytes for large scale lithium ion batteries. *Phys Chem Chem Phys* 2013;15:9145–55.
- [57] Sukhatme SP. A textbook on heat transfer. Hyderabad, India: Universities Press (India) Private Limited; 2005. p. 20.
- [58] Kim GH, Pesaran A. Battery thermal management system design modeling. In: Presented at the 22nd international battery, hybrid and fuel cell electric vehicle conference and exhibition (EVS-22), Yokohama, Japan; October 23–28, 2006.
- [59] Giuliano MR, Prasad AK, Advani SG. Experimental study of an air-cooled thermal management system for high capacity lithium-titanate batteries. *J Power Sources* 2012;216:345–52.
- [60] Gerardus S. Thermal management of hybrid electrical vehicles using heat pipes. Ph.D. Dissertation. Stellenbosch: Stellenbosch University; 2001 p.
- [61] Mills A, Farid M, Selman JR, Al-Hallaj S. Thermal conductivity enhancement of phase change materials using a graphite matrix. *Appl Therm Eng* 2006;26:1652–61.
- [62] Agynim F, Hewitt N, Eames P, Smyth Mervyn. A review of materials, heat transfer and phase change problem formulation for latent heat thermal energy storage systems (LHTESS). *Renew Sustain Energy Rev* 2010;14:615–28.
- [63] Al-Homoud MS. Performance characteristics and practical applications of common building thermal insulation materials. *Build Environ* 2005;40:353–66.
- [64] TIAC Mechanical insulation best practices guide, Section 2: Insulation materials and properties, pp. MP- revised 2013. <[http://tiac.ca/downloads/best-practices-guide/BestPracticesGuide\\_E.pdf](http://tiac.ca/downloads/best-practices-guide/BestPracticesGuide_E.pdf)>; (accessed in 01.01.15).
- [65] Baetens R, Jelle BP, Gustavsen A. Aerogel insulation for building applications: a state-of-the-art review. *Energy Build* 2011;43:761–9.
- [66] Datasheet: Pyrogel® XT, flexible industrial insulation for high-temperature applications. <<http://www.aerogel.com/products-and-solutions/all-insulation-products/>> (accessed in 01.01.15).
- [67] D.R. Lide. CRC Handbook of Chemistry and Physics, 74th edition, 2003, pp. 12–126.
- [68] Pye AM. A review of asbestos substitute materials in industrial applications. *J Hazard Mater* 1979;3:125–47.
- [69] Hermann WA, et al. US patent, US 8541126-B2, Tesla Motors Inc.
- [70] Hu HL, et al. US patent, US 8785026-B2, Industrial Technology Research Institute. Thermal runaway propagation model for designing a safer battery pack with 25 Ah  $\text{LiNi}_{1/3}\text{Co}_{1/3}\text{Mn}_{1/3}\text{O}_2$  large format lithium ion battery.